

1-1-2008

Synthesis and characterization of bulk and thin film antimony-selenium phase change alloys

Nirup Bandaru
University of Nevada, Las Vegas

Follow this and additional works at: <https://digitalscholarship.unlv.edu/rtds>

Repository Citation

Bandaru, Nirup, "Synthesis and characterization of bulk and thin film antimony-selenium phase change alloys" (2008). *UNLV Retrospective Theses & Dissertations*. 2391.
<http://dx.doi.org/10.25669/fhco-y25h>

This Thesis is protected by copyright and/or related rights. It has been brought to you by Digital Scholarship@UNLV with permission from the rights-holder(s). You are free to use this Thesis in any way that is permitted by the copyright and related rights legislation that applies to your use. For other uses you need to obtain permission from the rights-holder(s) directly, unless additional rights are indicated by a Creative Commons license in the record and/or on the work itself.

This Thesis has been accepted for inclusion in UNLV Retrospective Theses & Dissertations by an authorized administrator of Digital Scholarship@UNLV. For more information, please contact digitalscholarship@unlv.edu.

SYNTHESIS AND CHARACTERIZATION OF BULK AND THIN FILM $\text{Sb}_x\text{Se}_{100-x}$
PHASE CHANGE ALLOYS

by

Nirup Bandaru

Bachelor of Technology
J.N.T. University, India
2006

A thesis submitted in partial fulfillment
of the requirement for the

**Master of Science Degree in Electrical Engineering
Department of Electrical and Computer Engineering
Howard. R. Hughes College of Engineering**

**Graduate College
University of Nevada, Las Vegas
December 2008**

UMI Number: 1463494

INFORMATION TO USERS

The quality of this reproduction is dependent upon the quality of the copy submitted. Broken or indistinct print, colored or poor quality illustrations and photographs, print bleed-through, substandard margins, and improper alignment can adversely affect reproduction.

In the unlikely event that the author did not send a complete manuscript and there are missing pages, these will be noted. Also, if unauthorized copyright material had to be removed, a note will indicate the deletion.

UMI[®]

UMI Microform 1463494

Copyright 2009 by ProQuest LLC.

All rights reserved. This microform edition is protected against unauthorized copying under Title 17, United States Code.

ProQuest LLC
789 E. Eisenhower Parkway
PO Box 1346
Ann Arbor, MI 48106-1346



Thesis Approval

The Graduate College
University of Nevada, Las Vegas

September 4, 2008

The Thesis prepared by

Nirup Reddy Bandaru

Entitled

Synthesis and Characterization of Bulk and Thin Film

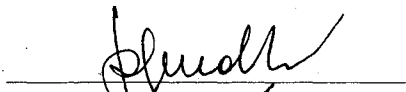
SbxSe100-x Phase Change Alloys

is approved in partial fulfillment of the requirements for the degree of

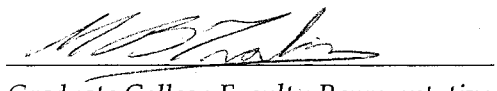
Master of Science in Electrical Engineering


Examination Committee Chair


Dean of the Graduate College


Examination Committee Member


Examination Committee Member


Graduate College Faculty Representative

ABSTRACT

Synthesis and Characterization of Bulk and Thin film $\text{Sb}_x\text{Se}_{100-x}$ Phase Change Alloys

by

Nirup Bandaru

Dr. Rama Venkat, Examination Committee Chair
Professor of Electrical and Computer Engineering
University of Nevada, Las Vegas

Dr. Ravhi S Kumar, Examination Committee Co-Chair
Professor of Physics and Astronomy
University of Nevada, Las Vegas

Phase change alloys have recently gained increasing attention due to their application in developing phase change random memory (PRAM) devices, as Flash memory based devices are rapidly approaching their technological limitations. The most dominant features of PRAM devices are its non-volatile nature, compatible with present day IC's manufacturing process, high density, fast operation, low power consumption etc.

Devices built on binary alloys such as Antimony – Selenium (SbSe) exhibit certain superior properties such as fast operation, reduced power consumption, economical etc. compared to that of ternary alloy (GST). In order to understand this behavior in detail, bulk $\text{Sb}_x\text{Se}_{100-x}$ ($40 \leq x \leq 70$) alloys are synthesized and deposited as thin films on silicon (100) plane substrate. Series of experiments such as X-ray diffraction analysis (XRD), Energy dispersive X-ray diffraction (EDAX), Spectroscopic Ellipsometer, Hall test experiments are carried out to characterize both the bulk and thin films. EDAX

experiments show the deviation between bulk and thin films compositions is less than 10%. Diffraction patterns of bulk exhibit orthorhombic structure, i.e., Sb_2Se_3 type where as thin films demonstrate amorphous behavior. Impact of annealing on thin films is studied by heating the films to 170°C under argon (Ar) ambience. Post annealing results of $\text{Sb}_{40}\text{Se}_{60}$ thin films show the crystal structure is orthorhombic and crystallization temperature (T_c) increases with increase in Sb content of the compound. Ellipsometry and Hall measurements of annealed films exhibit high refractive index (n), low extinction coefficient (k) and high carrier concentration with associated low carrier mobility. Further the conductivity of annealed $\text{Sb}_{40}\text{Se}_{60}$ thin films switches from p to n type.

TABLE OF CONTENTS

ABSTRACT.....	iii
LIST OF FIGURES	vii
LIST OF TABLES	ix
ACKNOWLEDGEMENTS.....	x
CHAPTER 1 INTRODUCTION	1
1.1 Categorization of the Thesis	2
CHAPTER 2 BACKGROUND	3
2.1 Devices Based on Phase Change Alloys.....	4
2.1.1 Trends in Optical Storage Technology	5
2.1.2 Phase Change Memory (PCM).....	6
2.1.2.1 Advantages and Limitations of PRAM.....	9
2.2 Chalcogenide Thin Film Fabrication	10
2.2.1 Physics of Thin Film Formation	10
2.2.2 Factors Affecting Thin Film Formation.....	12
2.2.3 Deposition Techniques.....	13
2.2.3.1 Thermal Evaporation	13
2.2.3.2 Sputtering.....	14
2.2.3.3 Chemical Vapor Deposition (CVD).....	15
2.3 Recent work on Chalcogenide Thin Films.....	15
CHAPTER 3 EXPERIMENTS.....	18
3.1 Synthesis and Characterization of Bulk SbSe.....	18
3.1.1 Bulk Samples Preparation.....	18
3.1.2 Characterization of Bulk Samples	19
3.1.2.1 X-ray Diffraction	19
3.1.2.2 Energy Dispersive X-ray Diffraction (EDAX) Analysis	21
3.1.2.3 Spectroscopic Ellipsometer.....	22
3.2 Thin Film Fabrication	23
3.2.1 Denton DV-502A Vacuum Evaporator System.....	24
3.2.2 Thin Film Characterization	26
3.2.2.1 Thickness Measurement.....	26
3.2.2.2 Compositional and Structural Analysis	27
3.2.2.3 Optical and Electrical Properties	27
3.2.2.3.1 Hall Test Equipment	28

3.2.2.4 Effect of Annealing.....	29
3.2.2.5 Post Annealing Analysis.....	29
CHAPTER 4 RESULTS AND DISCUSSIONS	30
4.1 Results and Discussions.....	30
4.1.1 Bulk.....	30
4.1.1.1 Compositional Analysis.....	30
4.1.1.2 Structural Analysis.....	31
4.1.1.3 Optical Constants.....	33
4.1.2 Thin Films.....	36
4.1.2.1 Thickness	36
4.1.2.2 Compositional Analysis.....	38
4.1.2.3 Pre/Post – Annealing	41
4.1.2.3.1 Structural Analysis.....	41
4.1.2.3.2 Optical Constants.....	41
4.1.2.3.3 Electrical Properties.....	52
4.2 Summary	56
CHAPTER 5 CONCLUSIONS AND FUTURE WORK.....	57
5.1 Conclusions.....	57
5.2 Future work.....	58
REFERENCES	59
VITA.....	62

LIST OF FIGURES

Figure 2.1	A schematic figure showing the spatial atomic arrangements of amorphous and polycrystalline materials. (a ₁), (b ₁) depicting the spatial atomic arrangement of amorphous and polycrystalline thin films and (a ₂), (b ₂) Surface reflectivity of amorphous and polycrystalline thin films.....	4
Figure 2.2	Technological trends in optical storage [9]	5
Figure 2.3	PRAM built on a thin film along with resistive electrode [12]	7
Figure 2.4	A Schematic diagram showing the phase transition, from amorphous to crystalline and crystalline to amorphous [15]	8
Figure 2.5	1-Transistor 1-Resistor model of a PRAM cell	9
Figure 2.6	Simplified model of thin film deposition [19]	12
Figure 2.7	Pictorial representations illustrating the difference between CVD and PVD	15
Figure 3.1	A schematic diagram showing X-ray diffraction from crystal planes with interplanar distance (d) [27]	20
Figure 3.2	A schematic representation of X-ray powder Diffractometer setup [28]	21
Figure 3.3	A photograph of the SEM – EPMA system used	22
Figure 3.4	A photograph showing a typical Spectroscopic Ellipsometer	23
Figure 3.5	A schematic diagram showing different parts Denton DV-502A Vacuum Evaporator system	24
Figure 3.6	An Interior view of the vacuum chamber	25
Figure 3.7	A typical Dektak II surface profilometer	26
Figure 3.8	Hall sample holder along with the thin film with four contacts	28
Figure 3.9	Photograph showing typical furnace and Quartz boat	29
Figure 4.1	X-ray Intensity versus 2θ plots for (a) Sb ₄₀ Se ₆₀ (b) Sb ₅₀ Se ₅₀ (c) Sb ₆₀ Se ₄₀ (d) Sb ₇₀ Se ₃₀	32
Figure 4.2	X-ray Intensity versus 2θ plots for various showing the in-situ high temperatures of Bulk Sb ₅₅ Se ₄₅ sample	33
Figure 4.3	Refractive index (n) and extinction coefficient (k) versus wavelength (λ) for the bulk Sb ₄₀ Se ₆₀	34
Figure 4.4	Plot of average refractive index (n) and extinction coefficient (k) as a function of Sb content	36
Figure 4.5	Thickness versus distance (d) between source and substrate of Sb ₄₀ Se ₆₀ thin films	38
Figure 4.6	Micro-structural images of Sb ₄₀ Se ₆₀ thin film obtained using SEM	39
Figure 4.7	(a) – (b) pre/post annealed X-ray Intensity versus 2θ plots for Sb ₄₀ Se ₆₀ thin film of 0.65 μm thickness	42
Figure 4.8	(a) – (b) pre/post annealed X-ray Intensity versus 2θ plots for Sb ₄₀ Se ₆₀ thin film of 1.00 μm thickness	43
Figure 4.9	(a) – (b) pre/post annealed X-ray Intensity versus 2θ plots for Sb ₅₀ Se ₅₀ thin	

	film of 0.525 μm thickness	44
Figure 4.10	(a) – (b) pre/post annealed X-ray Intensity versus 2θ plots for $\text{Sb}_{50}\text{Se}_{50}$ thin film of 1.70 μm thickness	45
Figure 4.11	(a) – (b) pre/post annealed X-ray Intensity versus 2θ plots for $\text{Sb}_{60}\text{Se}_{40}$ thin film of 0.30 μm thickness	46
Figure 4.12	(a) – (b) pre/post annealed X-ray Intensity versus 2θ plots for $\text{Sb}_{60}\text{Se}_{40}$ thin film of 1.66 μm thickness	47
Figure 4.13	(a) – (b) pre/post annealed X-ray Intensity versus 2θ plots for $\text{Sb}_{70}\text{Se}_{30}$ thin film of 0.20 μm thickness	48
Figure 4.14	(a) – (b) pre/post annealed X-ray Intensity versus 2θ plots for $\text{Sb}_{70}\text{Se}_{30}$ thin film of 0.60 μm thickness	49
Figure 4.15	Plot of average refractive index (n) and extinction coefficient (k) of pre and post annealed films as a function of Sb content.....	51
Figure 4.16	Plot of carrier concentration of pre/post annealed films as a function of Sb content	54
Figure 4.17	Plot of Mobility of pre/post annealed films as a function of Sb content.....	55

LIST OF TABLES

Table 2.1	Various optical storage media along with the wavelength of laser used, numerical operation storage capacity [10]	5
Table 4.1	Composition of Bulk samples obtained using EDAX	31
Table 4.2	Average optical constants of bulk samples	34
Table 4.3	Thicknesses of the deposited thin films for two distances for various compositions	37
Table 4.4	EDAX results of composition of various bulk and thin films and the % discrepancy between the results	40
Table 4.5	Pre/Post – annealed optical constants of film samples	50
Table 4.6	Pre/Post – annealed electrical parameters of thin film samples	53

ACKNOWLEDGEMENTS

I would like to thank Dr. Venkat for his invaluable suggestions and support throughout my thesis work and I feel privileged to have worked under him. Also, I would like to thank Dr. Ravhi for assisting and advising me throughout the research. My sincere gratitude goes to Dr. Paolo Ginobbi for his friendliness and helping hands. Also, I am grateful to Dr. Clay Crow for helping me with XRD and SEM. I would specially acknowledge Dr. Emma Regentova for serving as committee member and Dr. Mohamed B. Trabia for serving as graduate faculty representative. Finally, I would like to thank my friends for their constant encouragement.

CHAPTER 1

INTRODUCTION

Phase-change alloys also referred as Chalcogenide glass are gaining increasing interest because of their use in the data storage media, which is crucial to the information technology industry [1]. Compounds containing one or more chalcogenide elements such as Sulphur, Selenium, and Tellurium as a substantial component are known as Chalcogenides. These materials exhibit fast reversible amorphous-to-crystal phase transitions upon application of heat and can be used in applications as diverse as, non-volatile memory, optical disks, polarized holograms, opto-mechanical actuators and infrared optical waveguides [2].

The modern day technology is strongly associated with the advancement in data storage technology. Researchers are trying to find new approach and materials to build memory, which is non-volatile in nature, compatible with present day's IC manufacturing process, fast, dense, low power consumption, and economical [3]. One such promising candidate is Phase change Random Access Memory (PRAM) [4]. Thin films comprising chalcogenides are used in PRAM devices which upon application of heat switches state. The phase transition is accompanied by a change in electrical property, i.e., from highly resistive amorphous state to low resistance crystalline state. The interesting behavior of chalcogenide thin films is that apart from change in electrical and physical properties, they do undergo a change in optical properties during phase transitions. This feature is

exploited in writing and rewriting binary data onto optical media, compact disc (CD) and digital video disc (DVD). Potential phase change memory alloys are: GaSb, SbSe, InSb, InSe, GaSeTe, GeSbTe, AgInSbTe etc.

The most common commercially used chalcogenide alloy is GeSbTe (GST). But recent studies [5] on alloys containing Antimony (Sb) and Selenium (Se) show that SbSe has better scalability, lower melting point, low power consumption, fast speed of operation compared to that of GST. Hence this research focuses on synthesizing bulk SbSe alloy of varying compositions that is $\text{Sb}_x\text{Se}_{100-x}$ with increasing Sb content from 40% to 70%. Thin films of different thicknesses were fabricated out of bulk material using thermal evaporation technique. Characterization of bulk materials and thin films were done with respect to the structural, electronic and optical properties. Also compositional analysis was performed on bulk as well as thin films to make sure that the obtained composition is well within the design values. Finally the films were subjected to heat under argon gas ambience to study the affect of temperature on physical properties upon annealing. In addition to the above in-situ temperature x-ray diffraction (XRD) was carried out on bulk samples to see whether there is any crystal-structural transitions in the bulk upon heating.

1.1 Categorization of the Thesis

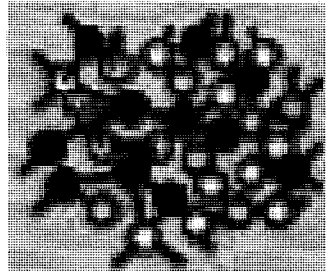
In chapter 2, a literature review on fabrication and characterization of different phase change materials is presented. Chapter 3 deals with the tools and experimental procedure used to characterize the samples, followed by results and discussion section in chapter 4. Conclusions and recommendations for future work are presented in chapter 5.

CHAPTER 2

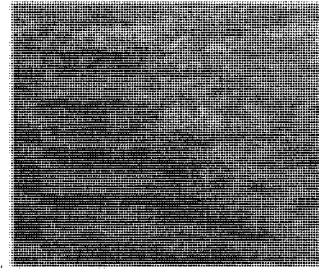
BACKGROUND

The phase change phenomenon a property exhibited by chalcogenide glasses was first explored as a potential memory technology by Stanford Ovshinsky of Energy Conversion Devices in the 1960s [5]. In the September 1970 issue of Electronics, Gordon Moore co-founder of Intel published an article on this technology [6]. However issues such as material quality and power consumption prevented commercialization of the technology. More recently, interest and research have resumed on chalcogenide thin films as flash and DRAM memory technologies are encountering scaling difficulties as chip lithography shrinks [7].

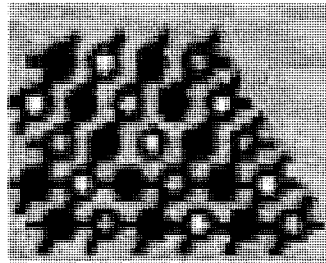
Phase change alloys have two stable states, i.e., amorphous and crystalline state. In amorphous phase, it is highly disordered, i.e., atoms in the material do not have particular spatial arrangement. In this state, the material displays high resistivity and high reflectivity. On the other hand, in crystalline or polycrystalline state, the material has well defined spatial atomic arrangement as shown in Figure 2.1 and exhibits low resistivity and low reflectivity [8].



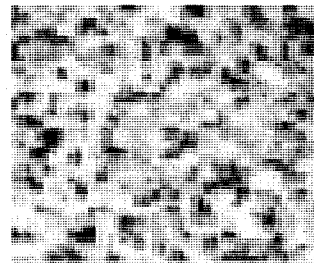
(a₁)



(a₂)



(b₁)



(b₂)

Figure 2.1 A schematic figure showing the spatial atomic arrangements of amorphous and polycrystalline materials. (a₁), (b₁) depicting the spatial atomic arrangement of amorphous and polycrystalline thin films and (a₂), (b₂) Surface reflectivity of amorphous and polycrystalline thin films.

2.1 Devices Based on Phase Change Alloys

Exploiting the change in optical properties between the amorphous and crystalline state, chalcogenide alloys are used in variety of applications such as writing and reading out data onto optical disks. Further, the change in electrical resistance of these material during phase transition is used new solid state memory device know as Phase Change Memory (PCM).

2.1.1 Trends in Optical Storage Technology

Re-writable compact discs (CD-RW) contains a phase-change alloy recording layer composed of a phase change material, most often AgInSbTe, an alloy of silver, indium, antimony and tellurium. An infrared laser beam is used to selectively heat and melt the crystallized recording layer into an amorphous state or to anneal it at a low temperature back to its crystalline state. The differences in reflectance of these areas can be used to detect digital information stored in compact discs (CD) [9]. Microstructurally these digital bits appear as pits and lands of size dictated by the spot size of the laser beam used for writing. With the growing needs of nonvolatile memory, it is desirable to have more information stored per square centimeter (sqcm). The amount of information stored on the disc is inversely proportional to the size of data spots (pits). The size of pits can be reduced by cutting down the wavelength of the laser beam used for writing. The technological trends in optical media [10] are illustrated in Figure 2.2.

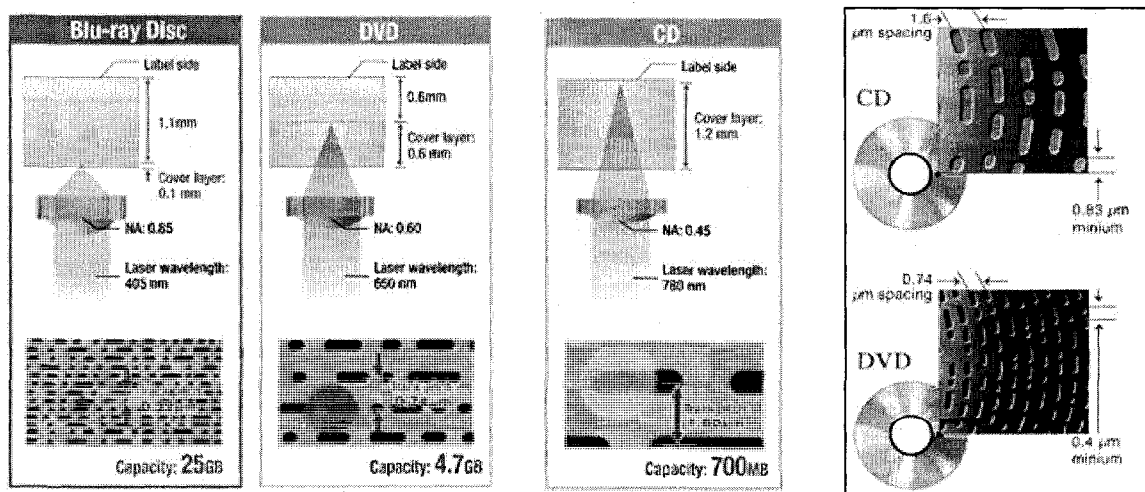


Figure 2.2 Technological trends in optical storage [9]

The size of the pits can also be reduced by increasing the size of the optical system's numerical aperture (NA), thereby the density of data stored can be increased dramatically as in blu ray discs. Effect of numerical aperture (NA) through wavelength on the amount of data stored onto optical discs is illustrated by the data presented in Table 2.1.

Table 2.1 Various optical storage media along with the wavelength of laser used, numerical operation storage capacity [10].

System	Wavelength (nm)	NA	Capacity (GB)
CD-RW/PD	780	0.45-0.50	0.65
DVD-RW/RAM	650	0.60-0.65	4.7
DVR-red	650	0.85	9.2
DVR-blue	400	0.85	21.5

It is noted that as the wavelength of laser is decreased the numerical aperture and proportionally the storage capacity increases.

2.1.2 Phase Change Memory (PCM)

As FLASH memory scaling trend is slowing down, there is a need for alternatives, which have relatively better trade off between scalability and reliability. One such promising technology is Phase Change Memory (PCM). Chalcogenide films exhibit negative resistance and bistable behavior and this property is used in the PCM technology. Dewald introduced the concept of PRAM in 1962, however, it was in early 2000s that the semiconductor industry started developing PCM on large scale [11]. In case of PRAM chip, the resistive electrode is used for heating of chalcogenide thin films to change the state from crystalline to amorphous chalcogenide, thus, changing the resistance of the film locally [12].

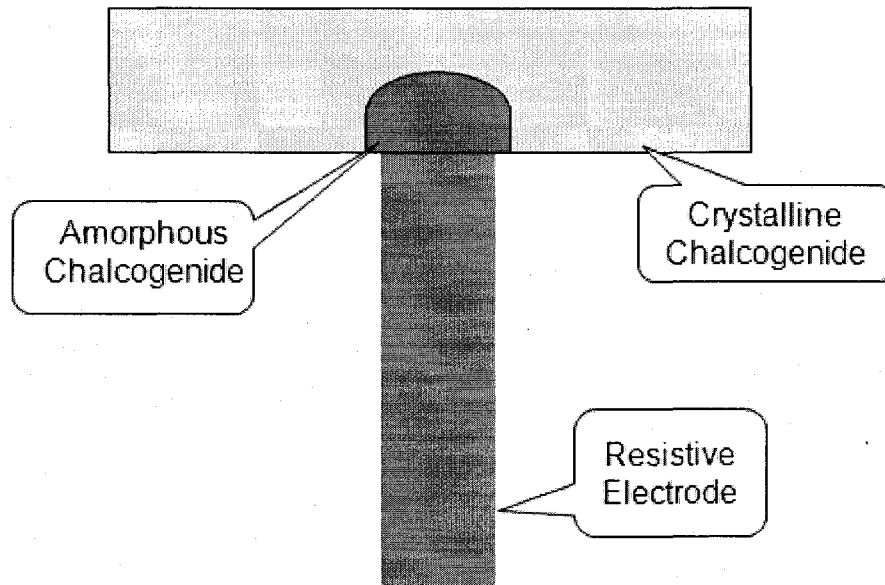


Figure 2.3 PRAM built on a thin film along with resistive electrode [12]

The chalcogenide thin film can be viewed as a variable resistor, hence the basic cell of PRAM can be modeled as a 1-transistor 1-resistor cell [13]. Programming is achieved by driving a current pulse through the resistive electrode so that the material, which is in close contact with the electrode, gets heated to a temperature higher than its melting temperature (T_m). The molten matter is super cooled by passing a trailing edge current pulse that last for a few nanoseconds only. Since the molten material has no time to rearrange the atomic bonds, it is left to be in amorphous state. The resistance of the amorphous chalcogenide is in the range of few mega ohms ($M\Omega$) and this state is referred to as “reset” state. In order to have the opposite transition, i.e., from amorphous to crystalline phase, a current pulse is passed through the electrode so that the material gets heated to a temperature which is less than its melting temperature (T_m) and then cooled

down slowly so that the material takes its original form, i.e., crystalline phase. The crystalline phase is referred to as “set” state, which has low resistance, i.e., in the range of few hundred to kilo ohms ($K\Omega$). The process of state of matter changes from crystalline to amorphous and then back to crystalline as a function of temperature is illustrated schematically in Figure 2.4 [13 -14].

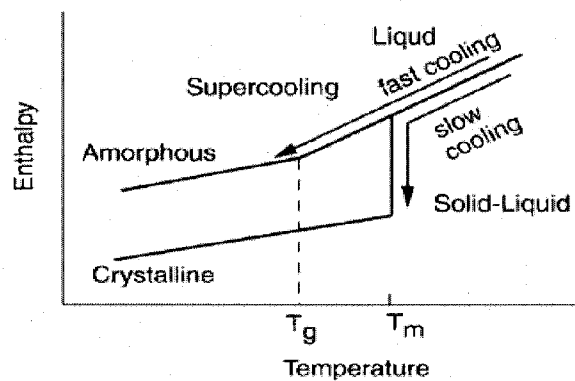


Figure 2.4 A Schematic diagram showing the phase transition, from amorphous to crystalline and crystalline to amorphous. [15]

Reading is accomplished by sensing the current flowing through cell under bias conditions. Under “set” state device the drive the bit line capacitances, thus, making it read to read a current through sense amplifier, which is represented as binary "1". A cell in “reset” state will not be able to trigger the sensing amplifier and hence does not read a current represented as binary "0" [15].

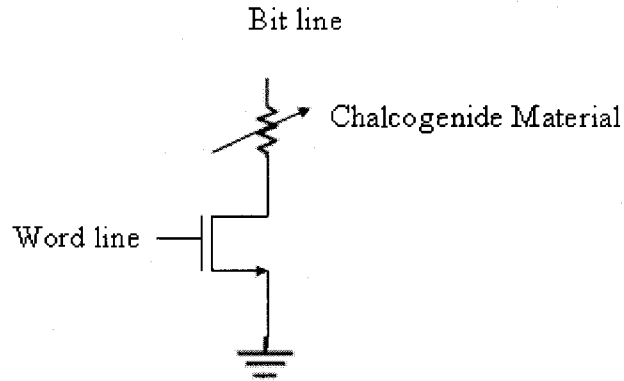


Figure 2.5 1-Transistor 1-Resistor model of a PRAM cell

2.1.2.1 Advantages and Limitations of PRAM

The following are the advantages of PRAM:

- Non-volatile in nature
- simple to design and compatible with the shrinking lithography
- Low writing times
- Better endurance characteristics
- Low power consumption
- Multi-bit capability and
- Economical

Although PRAM is one of the promising next generation non-volatile memory devices, there are a few limitations, which have to be addressed. PCM has high reset current, i.e., programming current density in the active region, which is greater than 10^7 A/cm² in most of the cases. This led the incorporation of heat sinks along with the cell so that the effect of the temperature on adjacent cells is reduced which increases the cost per

unit. Therefore, better ways have to be devised for in order to reduce the processing cost [16]. In addition, as phase change is a thermally driven process rather than electronic process care must be taken regarding the ambient conditions, otherwise data stored can be lost permanently.

2.2 Chalcogenide Thin Film Fabrication

In the section 2.1, possible applications of chalcogenide thin films were presented. GeSbTe and AgInSbTe are commonly used chalcogenide thin films, new materials with better performance characteristics are essential for developing this area of device applications further led to the fabrication of thin films of different compounds with varying compositions and characterizing them with respect to the physical, electronic, and optical properties.

2.2.1 Physics of Thin Film Formation

A solid material is said to be in thin film form when it is built up, as a thin layer on a solid support, called substrate, *ab initio* [17] by controlled condensation of the individual atomic, molecular, or ionic species, either directly by a physical process or through a chemical process.

Thin films are different from bulk materials in the following ways.

- Thin films are not fully dense
- Have a two dimensional (2-D) structure
- Strongly influenced by surface and interface effects
- Subject to stress, from lattice misfits with the substrate or difference in thermal characteristics between thin film and substrate exhibit different defect structure.

Thin film deposition process mainly involves the following three steps:

- Emission of atomic, molecular, or ionic particles from source (target) either through heat or physical sputtering by the other atomic species.
- Transport of these emitted particles to the substrate, which can be either directed or through vacuum.
- Condensation of particles on substrate, either directly or through a chemical reaction to form a solid deposit.

Formation of thin film takes place via nucleation and growth, details of which are presented below.

- The particles on impinging the substrate lose enough thermal energy to stay physically on the surface of the substrate. These adsorbed particles are known as adatoms. Typically, in this case the adatoms are attached to the surface through Van der Waal type bonding which has energies less than 0.3eV [18].
- The adatoms move over the surface by hopping from one location to another with help of thermal energy known as surface migration. During this process they interact with the other adatoms to form bigger clusters.
- These adatoms being thermodynamically unstable tend to desorb depending upon the deposition parameters such as flux rate and temperature. If the adatom reaches a stable cluster before getting desorbed, it enlarges the cluster.
- Since these clusters critical nuclei are less mobile and thermally stable than individual adatoms they tend to remain at the locations where they are formed and grow in size and numbers. These are called islands [18].
- In order to reduce the surface area these small islands start fusing with each other

to form bigger islands, known as agglomeration [18].

- These large islands continue to grow leaving behind channels or holes of exposed substrate leading to the formation of thin film.

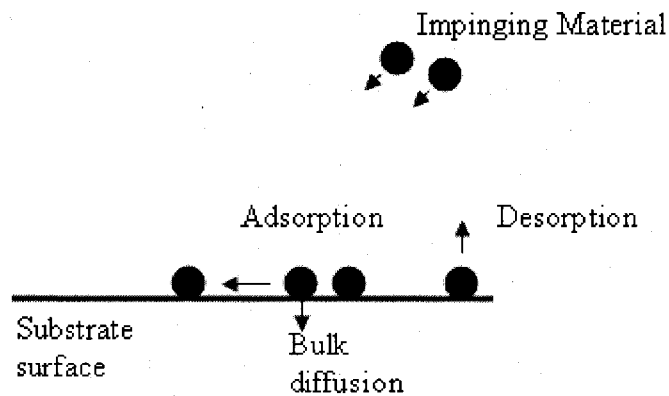


Figure 2.6 Simplified model of thin film deposition [19]

2.2.2 Factors Affecting Thin Film Formation

The following affect the formation of thin films.

- Deposition techniques
- Type of material to be deposited
- Substrate properties, which determine the amount of adhesion between the substrate and target atoms and the lattice misfits between the thin film and substrate.
- Surface irregularities of the substrate
- Rate of deposition and
- Medium such as argon gas, or vacuum.

2.2.3 Deposition Techniques

There are many ways to deposit a specimen as a thin film. The most commonly used one are Vapor deposition techniques. Vapor deposition techniques can be broadly divided into two categories:

- Physical Vapor Deposition (PVD) and
- Chemical Vapor Deposition (CVD)

Physical vapor deposition (PVD) is a vaporization coating technique, which involves transfer of solid material from the source to the substrate on an atomic level in a vacuum. The level of vacuum should be such that the mean free path of the target molecules is greater than the chamber dimensions and the distance from source to the substrate [18 - 19]. Furthermore physical vapor deposition technique can be classified as:

- Thermal Evaporation and
- Sputtering

2.2.3.1 Thermal Evaporation

Thermal evaporation known, as vacuum evaporation is one of the most widely used deposition techniques. As the name suggests, this technique consists of vaporization of the solid material by thermally heating the raw material above its melting temperature and then, condensing it onto a cooler substrate to form thin film. An electric resistance heater in the form of tungsten filament or a boat is used to heat the source material. This process is carried out in vacuum so that the material in the form of vapor reaches the substrate without scattering against any other gas atoms and also to avoid the presence of impurities. Molecular Beam Epitaxy (MBE) is a sophisticated form of thermal evaporation [15-18].

2.2.3.2 Sputtering

Sputtering is a PVD process in which the target atoms or molecules are ejected by bombarding the solid material with energetic and non-reactive ions. Usually argon gas (Ar) is used for bombarding the target. These ions upon impinging the solid material transfer energy and momentum to the target atoms, which condense on a substrate to form thin film. There should be enough ions, i.e., Ar plasma inside the deposition chamber in order to sustain the sputtering process [15-18].

Sputtering process is characterized by a parameter called sputter yield (S).

$$S = \text{number of ejected target atoms} / \text{number incident (Ar) ions}$$

Sputtering yield (S) depends upon:

- Type of sputtering employed
- Mass and energy of sputtering gas atoms
- Target materials which include the mass and binding energy of target atoms
- Geometry of the deposition chamber

Using magnetron sputtering, in which a magnetic field is used to yield multiple sputtering events by the ions, can enhance sputtering yield.

2.2.3.3 Chemical Vapor Deposition (CVD)

Chemical vapor deposition (CVD) is a process by which solid thin films are deposited on substrate by reacting vapor or liquid phase chemicals that contain the constituents of thin film. The main difference between CVD and PVD is that in PVD the target material is in solid form where as in CVD it can be either a liquid or a gas. A pictorial representation illustrating the difference between CVD and PVD is shown in Figure 2.7

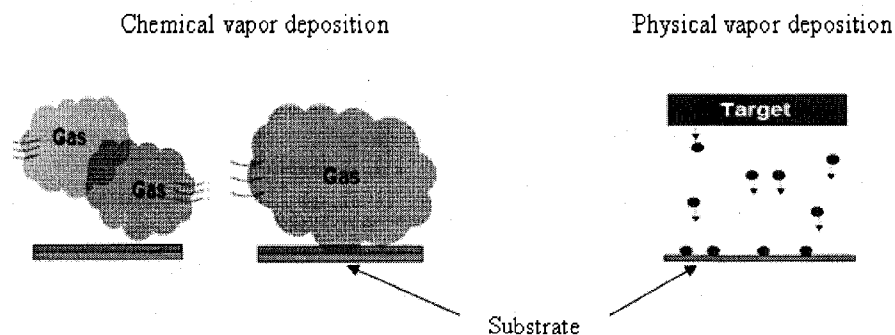


Figure 2.7 Pictorial representations illustrating the difference between CVD and PVD

2.3 Recent Work on Chalcogenide Thin Films

The growing demand for non-volatile memory and optical storage has resulted in search of new materials, which have better characteristics than the existing ones. Thin films of various materials are being fabricated and studied extensively with respect to the crystal structure, thermal stability, electronic properties etc. Although GST ($\text{Ge}_2\text{Sb}_2\text{Te}_5$) is the most commonly used phase change alloy, new methods have to be developed to increase its performance. One such effort is to study the effect of Silicon (Si) doping on electrical properties and thermal stability of GST thin films. It is observed that with the increase in silicon concentration both phase transition temperature and crystallization temperature increases but the melting point of the alloy decreases slightly. Also the electrical resistivity, i.e., dynamic resistance of the GST thin films increases with the Si content, which is suitable for phase change memory because of low writing (programming) current when compared to that of undoped GST films [20].

The impact of thickness of the film deposited is being studied with respect to the crystallization temperature and resistivity of the film. It is noted that thicker films crystallize more easily than thinner films and the film resistivity decreases with the

increase in the thickness of the film. Studies on GeSeTe_2 thin films fabricated through co-sputtering of individual elements in stoichiometric proportions proved out to be a good fit for PRAM devices because of their low phase transition temperature when compared to that of traditional $\text{Ge}_2\text{Sb}_2\text{Te}_5$ (GST) films [21].

Phase change alloys presented so far are either ternary or quaternary compounds with hazardous Tellurium (Te) as one of the primary constituent. Also fabricating these thin films with extremely good control over the balance of the individual elements is really difficult. So there is a need for new compounds, which can be fabricated with relatively more ease and free from Tellurium (Te), and hence environment friendly. Potential binary thin film alloys such as Antimony and Selenium (SbSe), Indium and Selenium (InSe), Silicon (Si) and Antimony (Sb) have gained increasing interest over the last few years because of their superior characteristics and the ease with which these can be fabricated compared to that of the traditionally used alloys.

The interesting feature of InSe thin film alloys is that the difference in the dynamic resistance between amorphous and crystalline phases is very high (greater than $10^5\Omega$). This avoids the concerns regarding the device failure due to phase decomposition and power consumption efficiency [22]. Recent studies on SbSe based thin film alloys such as $\text{Sb}_{65}\text{Se}_{35}$ show that these alloys have low melting temperature (T_m) and fast crystallization speed (t_c) over conventional GST thin films. Due to the reduction in the melting temperature (T_m), the resetting current required for SbSe based PRAMS devices is far less than that of GST based PRAMS, resulting in consumption of low power in SbSe PRAM devices. Further more, as these thin films undergo relatively fast phase transitions, devices based on them operate at high speeds. This extraordinary behavior of

SbSe based alloys led to the fabrication and study of $\text{Sb}_x\text{Se}_{100-x}$ ($40 \leq x \leq 70$) atomic weight percentage thin films with varying compositions. Thin films showed that the compound $\text{Sb}_{50}\text{Se}_{50}$ has the maximum crystallization temperature (T_c) [23 – 25].

CHAPTER 3

EXPERIMENTS

In this chapter, synthesis and characterization of bulk SbSe samples, which is the starting material for thin film deposition is discussed. Also the tools used for fabrication and characterization of $\text{Sb}_x\text{Se}_{100-x}$ thin film samples along with their necessary background details are discussed.

3.1 Synthesis and Characterization of Bulk SbSe

3.1.1 Bulk Samples Preparation

Bulk SbSe samples were synthesized using solid state reaction method. High purity (99.9%) Antimony (Sb) and Selenium (Se) metal powders obtained from Sigma-Aldrich were weighed in the appropriate ratio and thoroughly mixed in an agate mortar. The resultant product was pelletized using a dye and the pellets were introduced in a quartz tube. The quartz tube was flushed with purified Ar gas several times and evacuated to approximately 10^{-4} Torr. The quartz tube was then sealed and fired to 875°C in a box furnace. After 48h, the quartz tube was removed from the furnace and quenched to room temperature. Four different compositions of $\text{Sb}_x\text{Se}_{100-x}$ were placed in the same furnace simultaneously.

3.1.2 Characterization of Bulk Samples

The resultant ingot samples were characterized using X-ray diffraction (XRD) for crystal structure, Spectroscopic Ellipsometer for optical constants measurement and Energy Dispersive X-ray Analysis (EDAX) for composition analysis of each sample.

3.1.2.1 X-ray Diffraction

X-rays are electromagnetic radiation of wavelength about 1 Å, which is about the same size as an atom. Discovery of X-rays has enabled scientists to probe crystalline structure and chemical composition of different materials and thin films. Essentially X-ray diffraction has been used in two main areas, i.e., for the fingerprint characterization of crystalline materials and the determination of their structure. Each solid crystalline has its unique powder X-ray diffraction pattern, which can be used to determine the material structure [26]. X-ray diffraction is one of the most important characterization tools used in solid state material science.

The unit cell structure of any compound can be determined by analyzing the diffracted X-ray beams in accordance with the Bragg's law. Bragg's law is given by the equation 3.1 where 'd' is the interplanar distance, 'θ' is the angle of incidence with respect to the plane and 'λ' is the wavelength of the incident beam. As per Bragg's law, depending upon the path difference between the two reflected beams from inter planar atoms, they either add up constructively or destructively resulting in a intensity pattern on diffraction plates.

$$n(\lambda) = 2d\sin(\theta) \quad 3.1$$

By matching the incident angles of maximum intensity with that of known crystal structure, the crystal structure along with the lattice constants, which describe a unit cell,

can be obtained. The Figure 3.1 shows inter atomic planes between the atoms of a solid material.

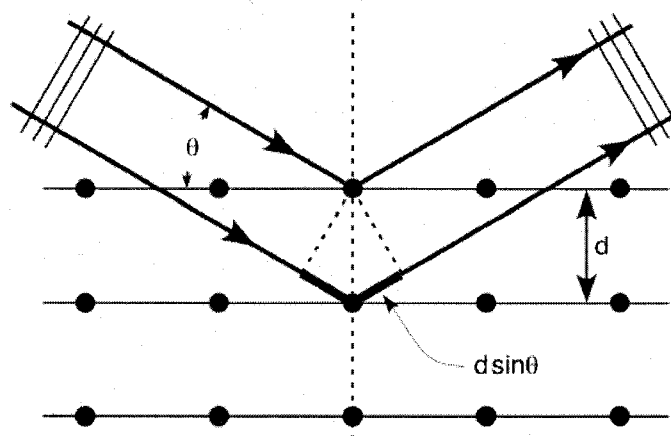


Figure 3.1 A schematic diagram showing X-ray diffraction from crystal planes with interplanar distance (d) [27].

Powder X-ray diffraction experiments were performed on the bulk $\text{Sb}_x\text{Se}_{100-x}$ samples, using PANalytical diffractometer operating with a Cu ($\text{K}\alpha$) radiation source. Also high temperature up to 120°C x-ray diffraction experiments were performed on $\text{Sb}_{55}\text{Se}_{45}$ bulk sample in an inert gas atmosphere, in order to study the stability of the bulk sample itself with respect to the temperature. A schematic figure showing the arrangement of the X-ray diffractometer is presented in Figure 3.2

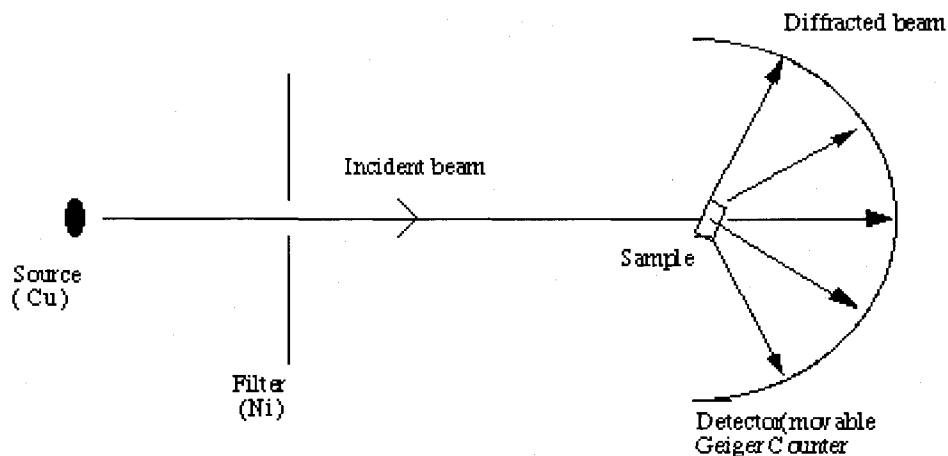


Figure 3.2 A schematic representation of X-ray powder Diffractometer setup [28]

3.1.2.2 Energy Dispersive X-ray Diffraction (EDAX) Analysis

EDAX also sometimes referred to as EDS analysis, is a technique used for determining the elemental composition of the specimen. The EDAX analysis system works as an integrated feature of a Scanning Electron Microscope (SEM), and can not operate on its own without the latter. In EDAX Analysis, the specimen to be analyzed is placed inside the SEM and bombarded with an electron beam. The bombarding electrons collide with the electrons of the specimen atoms, knocking some of them off in the process. During this process, an electron from outer electronic shell eventually occupies lower electronic shell vacated by an ejected inner shell electron. However, during this transition from high energy state to low energy state, the difference of energy between the two states is radiated as X-ray. Furthermore, the atom of every element releases X-rays with unique energy and hence wavelength during this process. Thus, by measuring the energy present of X-rays released by a specimen during electron beam bombardment, the identity of the atom from which the X-ray was emitted can be established, which is very useful in determining the composition of each element in a compound [29].

Composition of all bulk samples were obtained using a JOEL electron probe microanalyzer (EPMA) model JXA-8900 equipped with a scanning electron microscope model JSM-5610, a photograph of which is shown in figure 3.3.

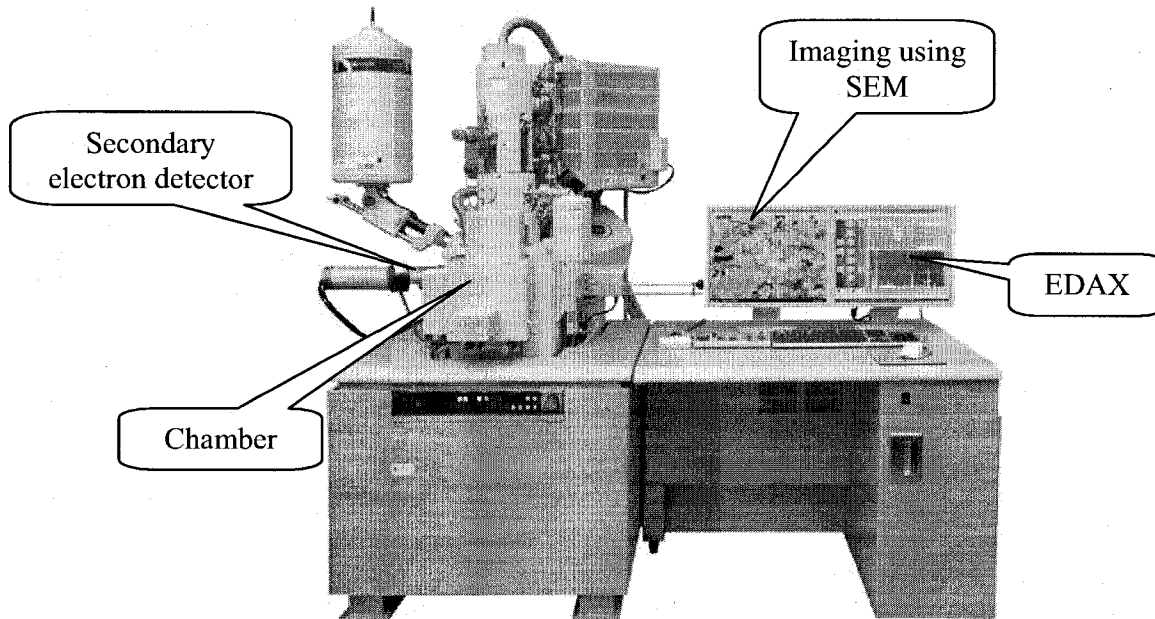


Figure 3.3 A photograph of the SEM – EPMA system used.

3.1.2.3 Spectroscopic Ellipsometer

Ellipsometry is a sensitive and powerful optical technique for the determination surface optical properties of thin films and bulk materials. As this is an optical technique, spectroscopic ellipsometry is non-destructive and contact less. Analyzing the change of polarization of light, which is reflected off a sample, one can determine the information regarding the thin film thickness and optical constants of the surface such as refractive index (n) and extinction coefficient (k) [30].

Hand polished bulk samples of the dimension $0.5 \times 0.5 \text{ cm}^2$ were analyzed using a variable angle Spectroscopic Ellipsometer (Model SE 200- Angstrom Sun Technologies Inc.). Optical light with wavelength in the range 300-800 nm was used as the incident beam. The angle of incidence was 75° to the normal of the sample. The intensity of the reflected wave as a function of wavelength was analyzed using standard software to obtain (n) and imaginary (k) part of refractive index of the four bulk samples. Figure 3.4 shows the experimental set up of a typical ellipsometer.

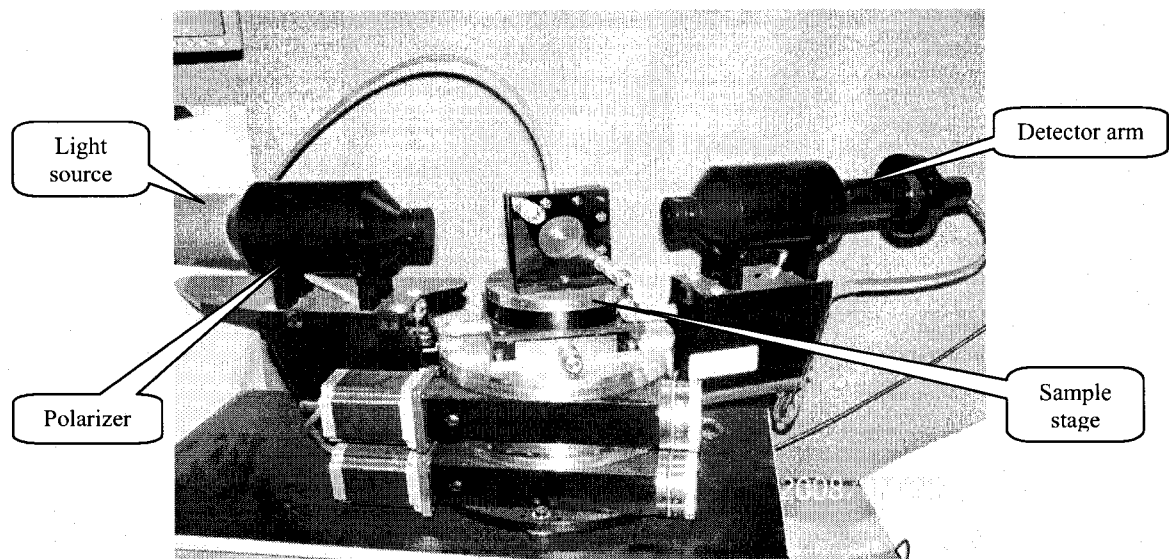


Figure 3.4 A photograph showing a typical Spectroscopic Ellipsometer

3.2 Thin Film Fabrication

Thin films of different compositions were deposited as thin films on Silicon (100) substrate using Denton DV-502A Vacuum System. A description of the system is presented below.

3.2.1 Denton DV-502A Vacuum Evaporator System

Denton vacuum system is a tool used for depositing thin films. The deposition is done through a physical deposition process (PVD). The Figure 3.5 is a schematic diagram of the main components of the vacuum system.

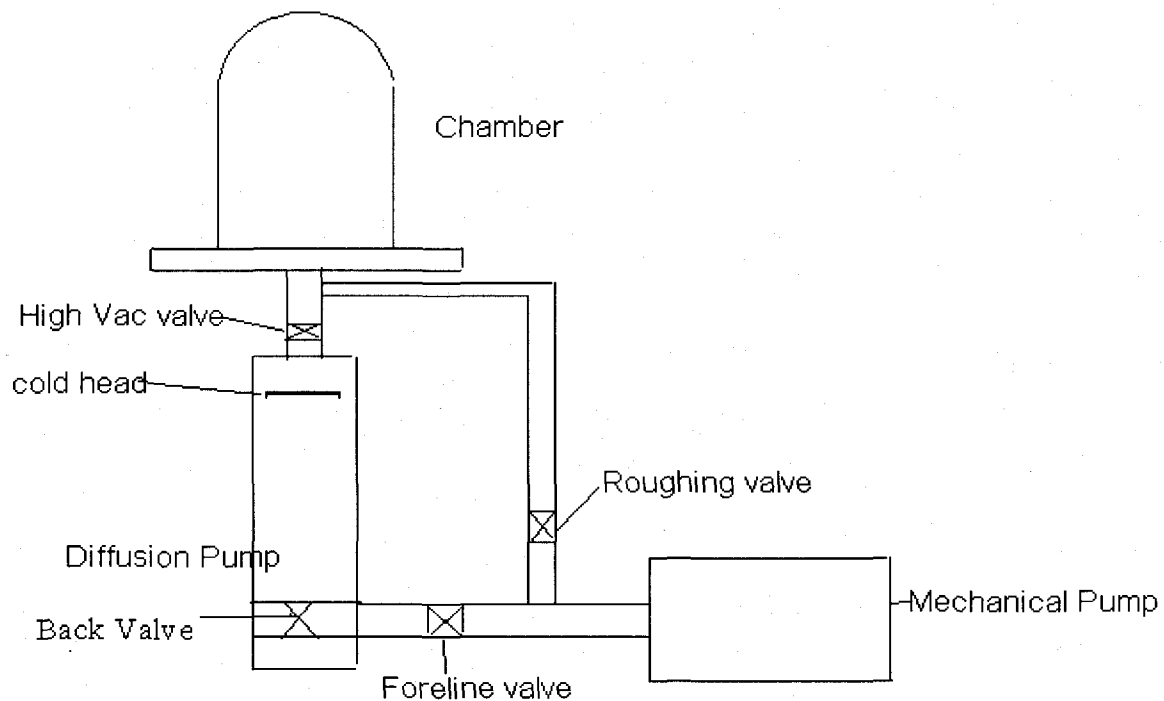


Figure 3.5 A schematic diagram showing different parts Denton DV-502A Vacuum Evaporator system

As shown in the Figure 3.5, it has a chamber which is connected to a pair of vacuum pumps, namely mechanical and diffusion pump. These pumps are coupled to each other and to the chamber through a set of valves, i.e., roughing, high vacuum, back, foreline

valves. To avoid any impurities during the deposition, the chamber was evacuated by running these pumps simultaneously, until a certain degree of desired vacuum level was achieved. The vent valve is closed during the deposition and usually used to vent the chamber to the atmosphere. Typically the best vacuum level that can be achieved in this equipment is around 10^{-5} torr.

Inside the vacuum chamber, there is a pair of electrodes connected through a resistive tungsten filament or basket. The bulk material (Target) to be deposited as thin film was placed inside this basket and heated to a temperature above its melting point, by passing current through the electrodes. During this process, the solid target evaporates and eventually condenses onto the cooler substrate, which was placed on the platen beneath the tungsten filament. The platen was not rotated during deposition. A interior view of the vacuum chamber showing the platen and the two electrodes is shown in the Figure 3.6.



Figure 3.6 An Interior view of the vacuum chamber

As mentioned earlier, in order to study the effect of film thickness on its properties, the substrates were placed at two different distances from the target. This was accomplished by using a series of aluminum plates each of thickness 0.6cm as shown in Figure 3.6. During deposition, a current of 42A was allowed to pass through the electrodes, the pressure inside the chamber was 9×10^{-5} torr. Since the time of deposition was only 3 seconds, it was estimated the platen could not even be rotated one time completely. Thus the platen was not rotated.

3.2.2 Thin Film Characterization

3.2.2.1 Thickness Measurement

The thicknesses of the as-deposited thin films were determined using Dektak II surface profilometer. The Dektak II Surface Profiler is a microprocessor-based instrument used for taking accurate measurements on small vertical profiles ranging in height from 100nm to 10,000nm. It obtains vertical profiles by the movement of a sensitive diamond tipped stylus over the substrate. The force with which the stylus moves over the substrate is around 60mg and can be adjusted. The vertical profile data is recorded and sent to the transducer for digitization and future plot manipulation [31].

This is a destructive way of measuring the thickness of a thin film, because due to the force exerted by the stylus on the surface of the film, the film structure and properties may change. In order to avoid this, a glass slide with step profile was created and the silicon substrate was mounted on it. Both the substrate and the slide were exposed for deposition. Neglecting the subtle variations in height of the glass slide and the substrate with respect to the target, the step profile obtained on the glass slide was used for

determining the thicknesses of the film deposited. Figure 3.7 shows a typical Dektak II profilometer used for measuring the thickness of thin films.

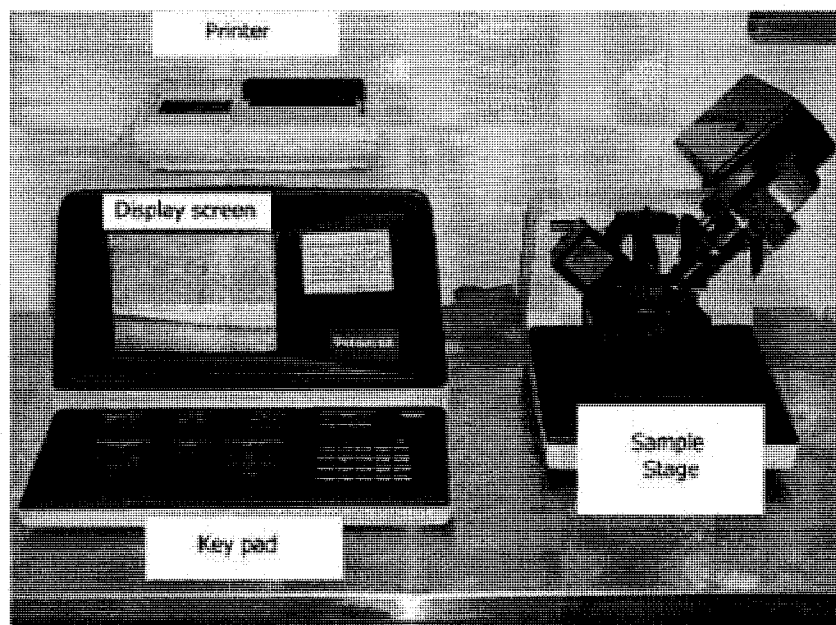


Figure 3.7 A typical Dektak II surface profilometer

3.2.2.2 Compositional and Structural Analysis

The compositions of the thin films, with varying thicknesses were determined by performing EDAX experiments on them. Also the structural analysis of the as-deposited thin films was determined using X-ray diffraction, which are already discussed in detail in section 3.1.2.1 and 3.1.2.2 respectively.

3.2.2.3 Optical and Electrical Properties

Optical properties of the thin films were determined using Spectroscopic Ellipsometer in similar fashion as done for bulk samples, discussed in section 3.1.2.3

Electronic properties of the thin film samples such as film resistivity, surface carrier concentration, conductivity type i.e., 'n' or 'p' type semiconductor etc. were determined using Keithley 920 series Hall Test Equipment.

3.2.2.3.1 Hall Test Equipment

The basic working of the Hall test equipment is based on the Hall Effect, discovered by E. H. Hall in 1879. According to this effect whenever an electric current flows through a conductor in presence of a magnetic field, the magnetic field exerts a transverse force on the moving charge carriers which tends to push them to one side of the conductor. To counteract this, there is buildup of charges at the sides of the conductors, thus creating a potential difference between the two sides of the conductor. The presence of this measurable transverse voltage is called the Hall Effect and is most evident in thin flat conductors and semiconductors [32].

As a part of experiment, the thin film sample was glued to the sample holder and four contacts were created at the corners of the film using gold and silver paints respectively. Later, the sample holder was placed between the poles of an electromagnet inside the hall chamber. The snapshot of the sample holder along with thin film is shown in Figure 3.8.

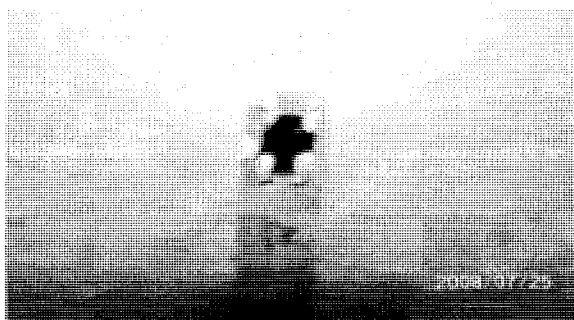


Figure 3.8 Hall sample holder along with the thin film with four contacts

3.2.2.4 Effect of Annealing

Effect of temperature annealing on thin film behavior such as structure, optical and electronic properties were carried by heating the samples under argon (Ar) ambient. The thin film samples were placed on a quartz boat as shown in the Figure 3.9 whose melting point is around 2000°C . Later, the boat was placed inside the High temperature tube furnace 54500 and heated to a temperature 170°C for 60 minutes, with the pressure of the tube being maintained at 695 torr constantly.

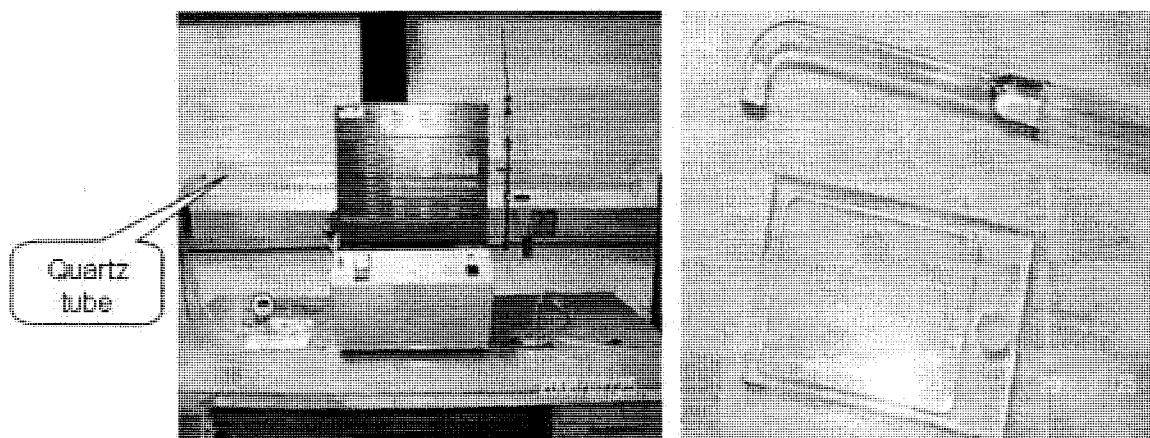


Figure 3.9 Photograph showing typical furnace and Quartz boat

3.2.2.5 Post Annealing Analysis

After annealing, structural analysis was performed on the thin film samples using X-ray diffractor to see any structural (physical) changes in the film, followed by determining the optical and electronic properties of the annealed samples as illustrated earlier.

CHAPTER 4

RESULTS AND DISCUSSIONS

SbSe bulk samples were synthesized and deposited as thin films on 100 plane Silicon (Si) substrate. Thin films deposition was carried out under the following conditions, current, $I = 42\text{A}$, pressure, $P = 9 \times 10^{-5}$ torr, and time of duration, $t = 3$ sec. Composition and structural of bulk and thin films was performed using Scanning Electron Microscope (SEM) and X-ray Diffractometer (XRD). Also bulk and thin film samples were characterized with respect to the optical and electrical properties using Spectroscopic Ellipsometer and Hall test equipment respectively.

4.1 Results and Discussions

4.1.1 Bulk

4.1.1.1 Compositional Analysis

Compositions of each bulk samples were verified using Energy Dispersive Analysis of X-rays system (EDAX) associated with JOEL JSM – 5600 Scanning Electron Microscope. The observed results were well within the designed values, with errors less than 12% as shown in Table 4.1.

Table 4.1 Composition of Bulk samples obtained using EDAX

S.No	Compound	% Atomic Composition				% Error	
		Designed Values		EDAX Results			
		Sb	Se	Sb	Se	Sb	Se
1.	$\text{Sb}_{40}\text{Se}_{60}$	40	60	44.88	55.12	12.22	8.13
2.	$\text{Sb}_{50}\text{Se}_{50}$	50	50	53.59	46.41	7.18	6.82
3.	$\text{Sb}_{60}\text{Se}_{40}$	60	40	55.49	44.51	7.51	11.80
4.	$\text{Sb}_{70}\text{Se}_{30}$	70	30	68.82	31.18	1.68	3.90

The variation between the designed value and EDAX value of composition can be attributed to vapor pressure difference between Sb and Se at the quenching temperature of 875°C.

4.1.1.2 Structural Analysis

Crystal structure of bulk samples were determined using X'Pert PRO PANalytical – Cu k (α) - 1.54 Å XRD machine, with voltage, V=40kV and current, I=30mA. The intensity versus 2θ plots of all four samples (listed in Table 1) show Sb_2Se_3 type structure, i.e., orthorhombic as shown in Figures 4.1 (a-d).

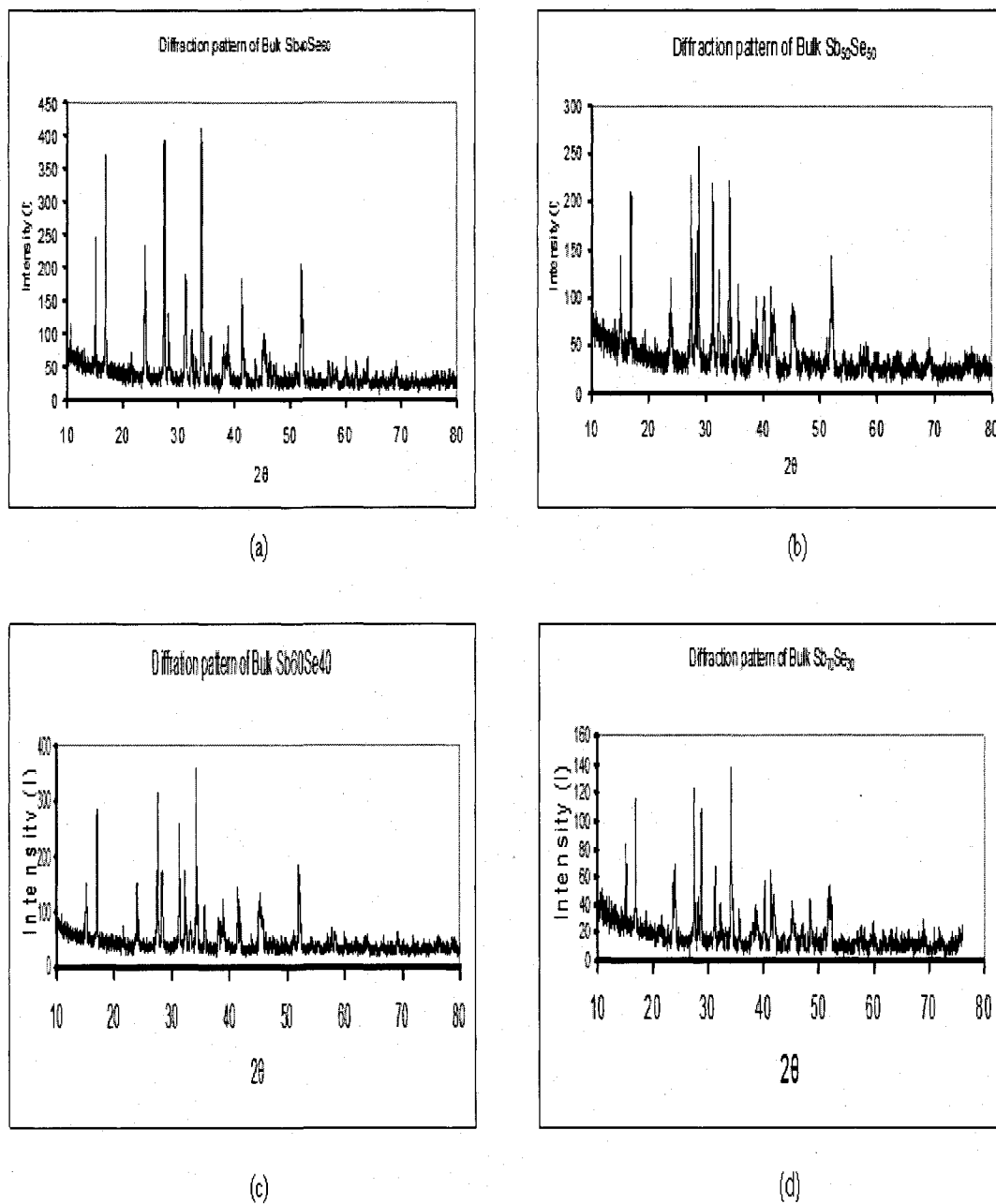


Figure 4.1 X-ray Intensity versus 2θ plots for (a) $\text{Sb}_{40}\text{Se}_{60}$ (b) $\text{Sb}_{50}\text{Se}_{50}$ (c) $\text{Sb}_{60}\text{Se}_{40}$ (d)

$\text{Sb}_{70}\text{Se}_{30}$

The stability of the crystal structures with respect to the temperature were determined using in-situ high temperature X-ray diffraction. Results presented in Figure 4.2 shows

that the room temperature bulk $\text{Sb}_{55}\text{Se}_{45}$ crystal structure, i.e., orthorhombic is stable at least up to 120°C . In-situ temperature in the XRD system could not be ranged beyond 120°C due to system limitations.

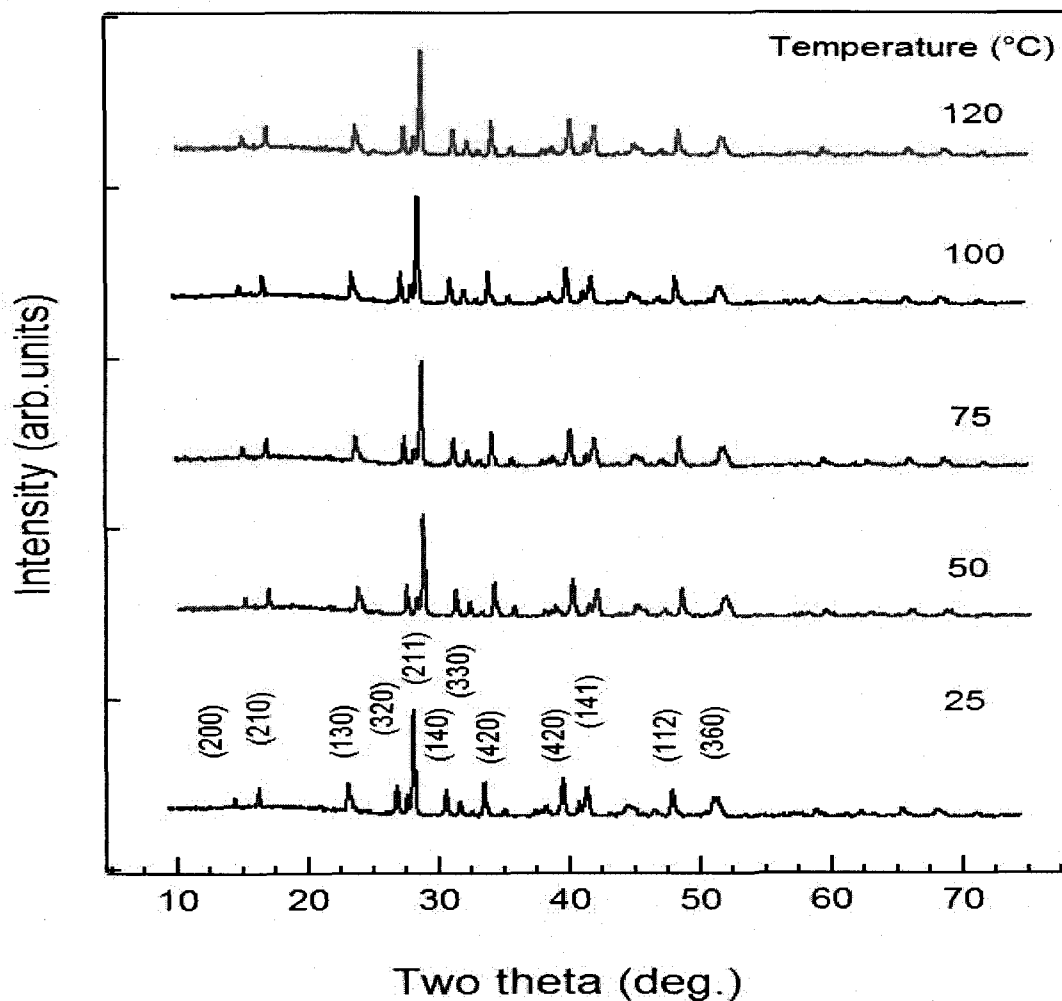


Figure 4.2 X-ray Intensity versus 2θ plots for various showing the in-situ high temperatures of Bulk $\text{Sb}_{55}\text{Se}_{45}$ sample.

4.1.1.3 Optical Constants

Optical constants of bulk compositions were determined using Spectroscopic Ellipsometer – Model: SE200 Angstrom Sun Technologies Inc. With the angle of incidence fixed at 75° refractive index (n) and extinction coefficient (k) of each bulk sample was obtained for a series of wavelengths ranging from 300 – 800 nm as shown in the Figure 4.3. Average values are calculated and tabulated in Table 4.2.

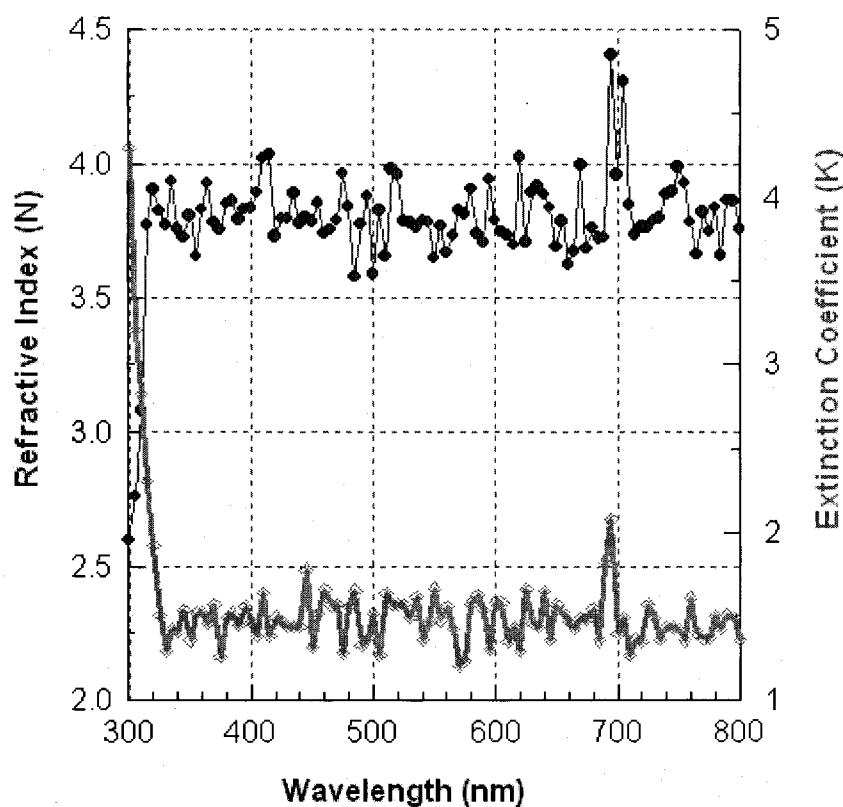


Figure 4.3 Refractive index (n) and extinction coefficient (k) versus wavelength (λ)
for the bulk $\text{Sb}_{40}\text{Se}_{60}$.

Table 4.2 Average optical constants of bulk samples.

S.No	Compound	Average Refractive Index (n)	Average Extinction coefficient (k)
1.	Sb ₄₀ Se ₆₀	3.95	1.13
2.	Sb ₅₀ Se ₅₀	4.0	1.28
3.	Sb ₆₀ Se ₄₀	6.23	0.83
4.	Sb ₇₀ Se ₃₀	5.79	1.61

The variation of average optical constants as a function of composition is shown in the Figure 4.4. It is observed that the average refractive index (n) increases with increase in Sb content from 3.95 at 40% of Sb to 6.23 at 60% of Sb and decreases slightly to 5.79 beyond that. The variation in average extinction coefficient (k) is random.

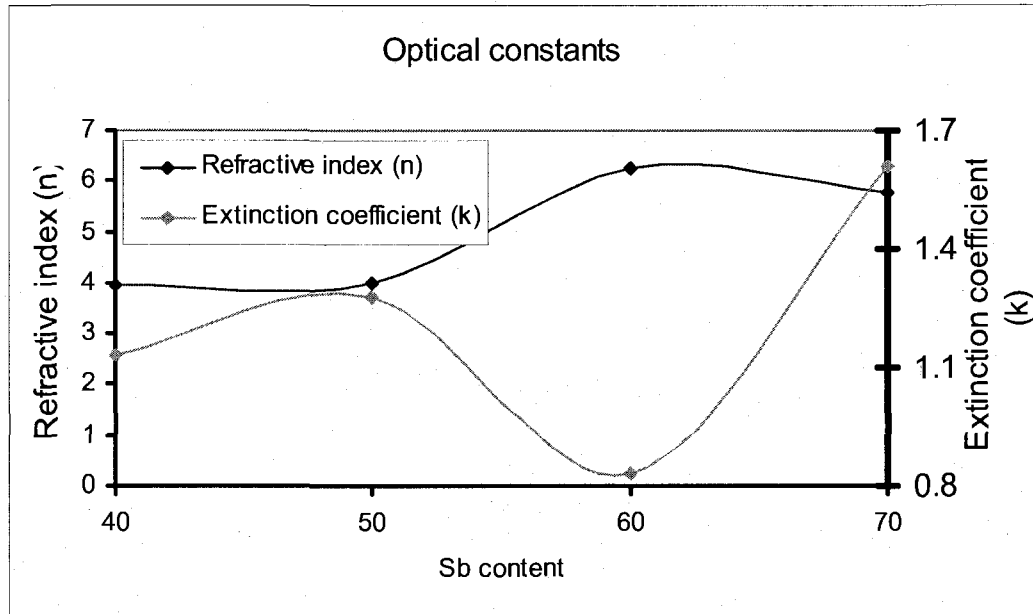


Figure 4.4 Plot of average refractive index (n) and extinction coefficient (k) as a function of Sb content.

4.1.2 Thin Films

4.1.2.1 Thickness

The bulk materials were deposited as thin films on (100) silicon substrate using Denton DV-502A vacuum system. As mentioned in chapter 3, thin films of two different thicknesses were deposited for every bulk target by varying the distance between the target and the substrate using Aluminum (Al) plates as mentioned in chapter 3. The distances used were $x = 3.7$ cm and $y = 2.9, 1.7$ cm respectively. The thicknesses of the two films were determined using Dektak II surface profiler and their variation as a function of distance from the substrate is shown in the Figure 4.5. The thickness has $1/d^2$ dependence where 'd' is the distance between the source and the substrate. Upon substituting the values of x and y in equation 4.1, distance (d) is calculated. The

thicknesses obtained for two different distances for various compositions are reported in Table 4.3.

$$d = \sqrt{x^2 + y^2} \quad 4.1$$

Table 4.3 Thicknesses of the deposited thin films for two distances for various compositions

S.No	Compound	Distance between the source and substrate, d in cm	Thickness in μm
1a.	$\text{Sb}_{40}\text{Se}_{60}$	4.701	0.65
1b.	$\text{Sb}_{40}\text{Se}_{60}$	4.071	1.00
2a.	$\text{Sb}_{50}\text{Se}_{50}$	4.701	0.525
2b.	$\text{Sb}_{50}\text{Se}_{50}$	4.071	1.70
3a.	$\text{Sb}_{60}\text{Se}_{40}$	4.701	0.3
3b.	$\text{Sb}_{60}\text{Se}_{40}$	4.071	1.66
4a.	$\text{Sb}_{70}\text{Se}_{30}$	4.701	0.2
4b.	$\text{Sb}_{70}\text{Se}_{30}$	4.071	0.6

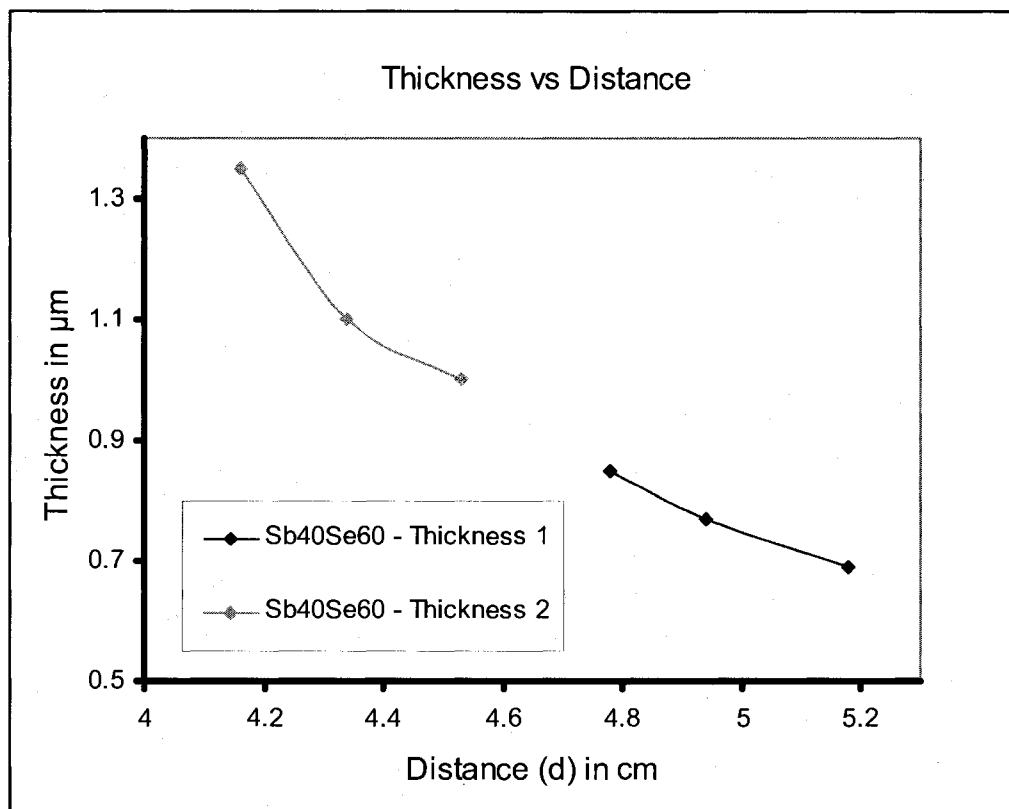


Figure 4.5 Thickness versus distance (d) between source and substrate of $\text{Sb}_{40}\text{Se}_{60}$ thin films.

4.1.2.2 Compositional Analysis

It is very crucial that for device applications the compositions of the deposited thin films are consistent with respect to the compositions of the bulk samples. This was verified by subjecting the thin film samples to EDAX analysis. The obtained results are presented in Table 4.4. From the data reported in Table 4.4, the discrepancy between the compositions of the bulk and thin films is less than 7%. This level of variation is acceptable as the thin film deposition is a evaporation technique, where differential vapor pressure at melting point may result in variation in composition. Apart from determining

the composition of films, Scanning Electron Microscope (SEM) was used to obtain the micro-structural images of the thin films which are shown in the Figure 4.4 respectively.

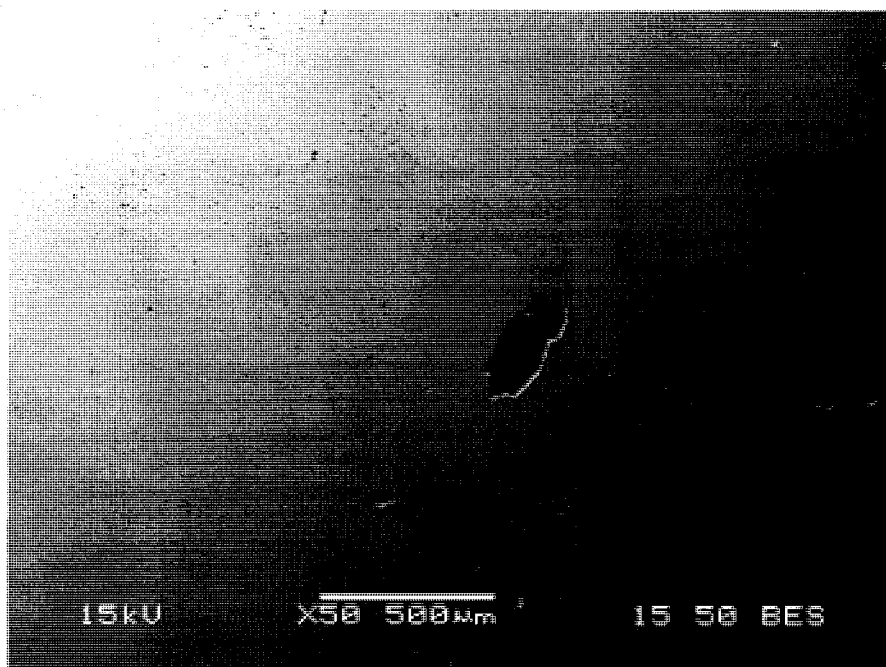


Figure 4.6 Micro-structural images of Sb₄₀Se₆₀ thin film obtained using SEM.

Table 4.4 EDAX results of composition of various bulk and thin films and the % discrepancy between the results.

S.No	Compound	EDAX results in %. Atomic Composition				%. Discrepancy	
		Bulk		Thin films			
		Sb	Se	Sb	Se	Sb	Se
1a.	Sb ₄₀ Se ₆₀	44.88	55.12	48.88	55.12	0	0
1b.	Sb ₄₀ Se ₆₀	44.88	55.12	43.05	56.95	4.07	3.30
2a.	Sb ₅₀ Se ₅₀	53.59	46.41	51.23	48.77	4.40	5.08
2b.	Sb ₅₀ Se ₅₀	53.59	46.41	51.46	48.54	3.97	4.58
3a.	Sb ₆₀ Se ₄₀	55.49	44.51	57.63	42.37	3.85	4.80
3b.	Sb ₆₀ Se ₄₀	55.49	44.51	58.24	41.76	4.95	6.15
4a.	Sb ₇₀ Se ₃₀	68.82	31.18	67.72	32.28	1.59	3.52
4b.	Sb ₇₀ Se ₃₀	68.82	31.18	68.28	31.72	0.78	0.16

From Figure 4.4, it is found that there are void spots on thin film surface indicating that the deposition is not uniform. This can be avoided by either slowing down the rate of deposition, i.e., increasing the time of deposition or by employing different deposition techniques such as Sputtering, Chemical Vapor Deposition (CVD) etc.

4.1.2.3 Pre/Post – Annealing

It is mentioned in chapter 3, that the thin films were annealed in order to study the effect of temperature on thin film properties such as crystalline structure, optical and electrical properties.

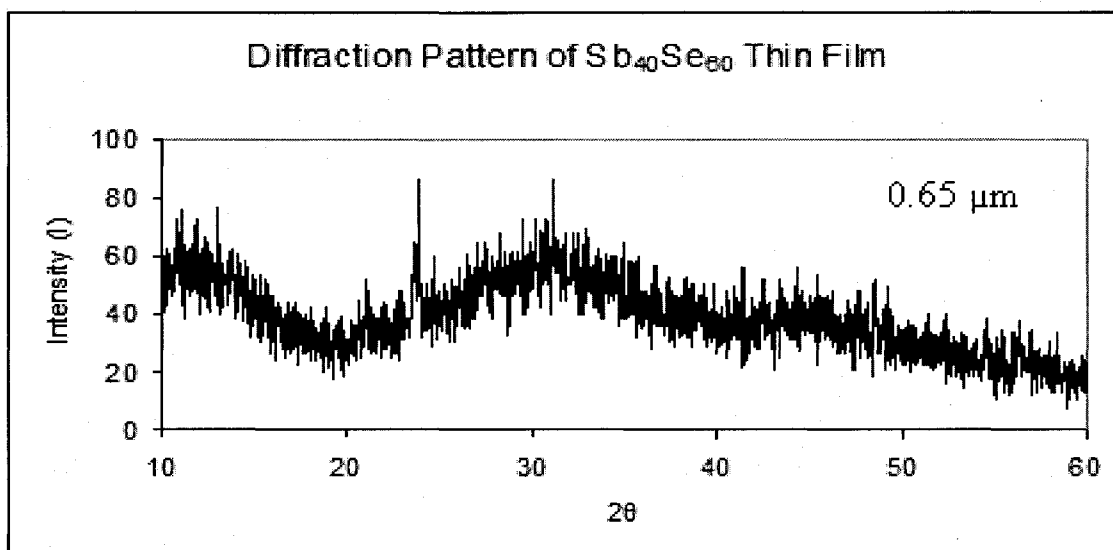
4.1.2.3.1 Structural analysis

XRD was performed on pre-annealed film samples and the obtained results are presented in the Figures 4.7 through 4.14.

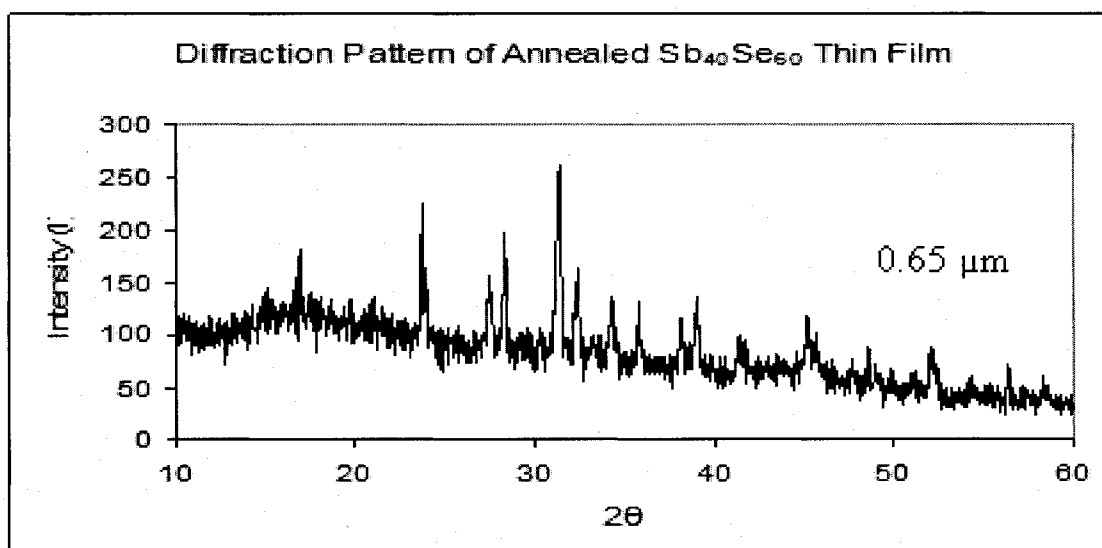
Pre/Post - annealing X-ray diffraction analysis of thin film samples show that of the four different compositions, only $\text{Sb}_{40}\text{Se}_{60}$ thin film sample of two different thicknesses crystallized to orthorhombic structure upon heating to 170°C as shown in the Figure 4.7 (a - b). This change in crystal structure is attributed to the phase transformation occurring in thin films upon application of heat energy. From the Figures 4.7 – 4.14, it is noticed that the crystallization temperature (T_c) for thin film compositions with higher Sb content ($> 40\%$) is greater than 170°C , i.e., the amount of heat energy required for phase transformation in these thin film compositions is higher than $\text{Sb}_{40}\text{Se}_{60}$ thin films.

4.1.2.3.2 Optical Constants

Optical constants n and k of pre/post - annealed films were determined using spectroscopic ellipsometer with the conditions being the same as mentioned in section 4.1.1.3. The obtained optical parameters are illustrated in the Table 4.5.

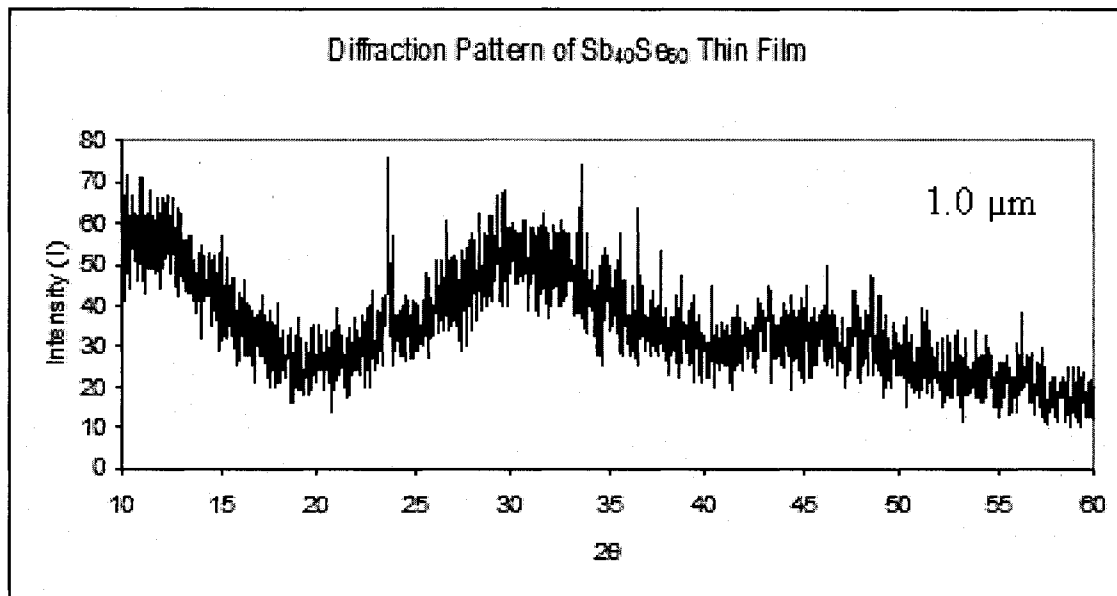


(a)

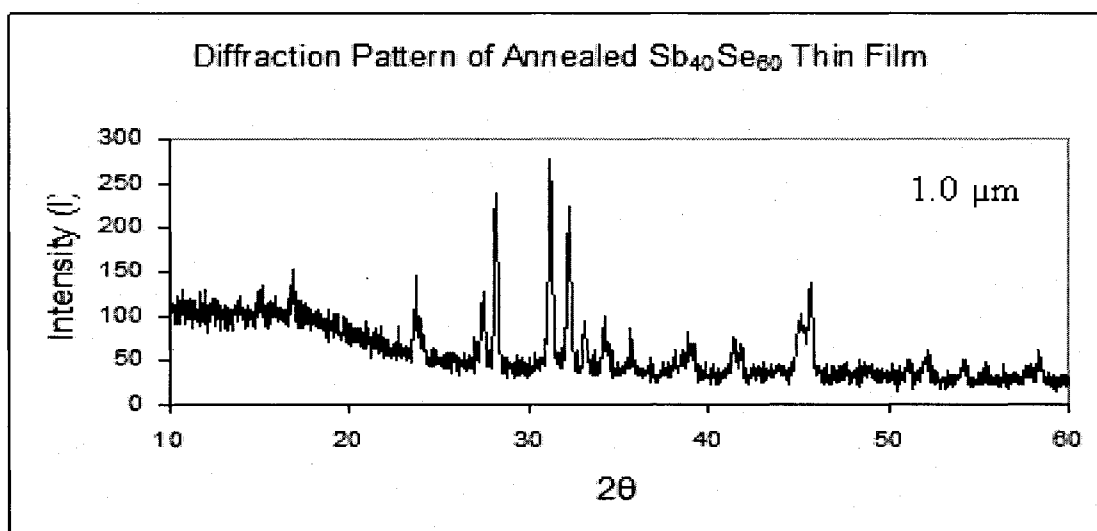


(b)

Figure 4.7 (a) – (b) pre/post annealed X-ray Intensity versus 2 θ plots for $\text{Sb}_{40}\text{Se}_{60}$ thin film of 0.65 μm thickness.

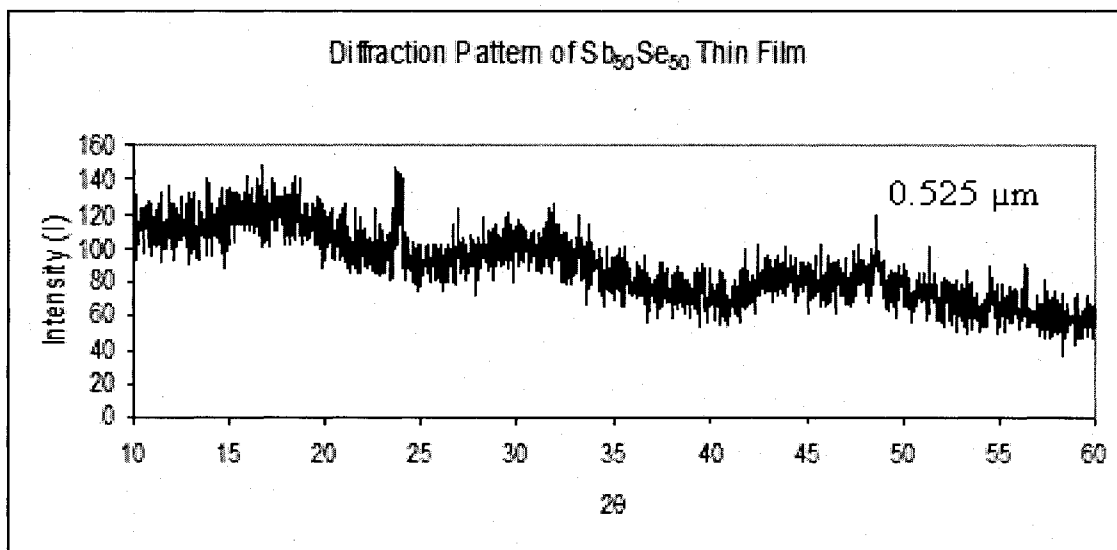


(a)

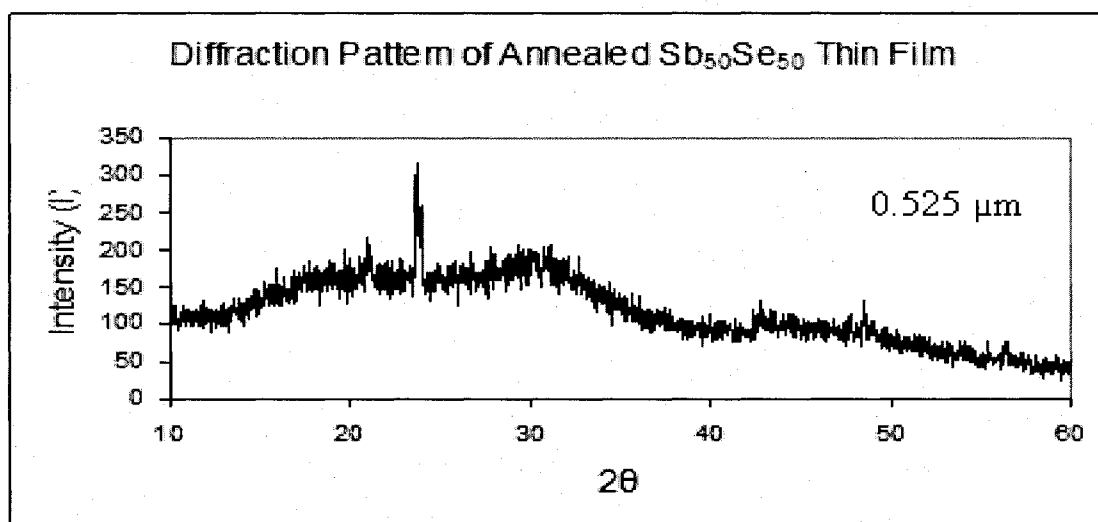


(b)

Figure 4.8 (a) – (b) pre/post annealed X-ray Intensity versus 2θ plots for $\text{Sb}_{40}\text{Se}_{60}$ thin film of 1.00 μm thickness.

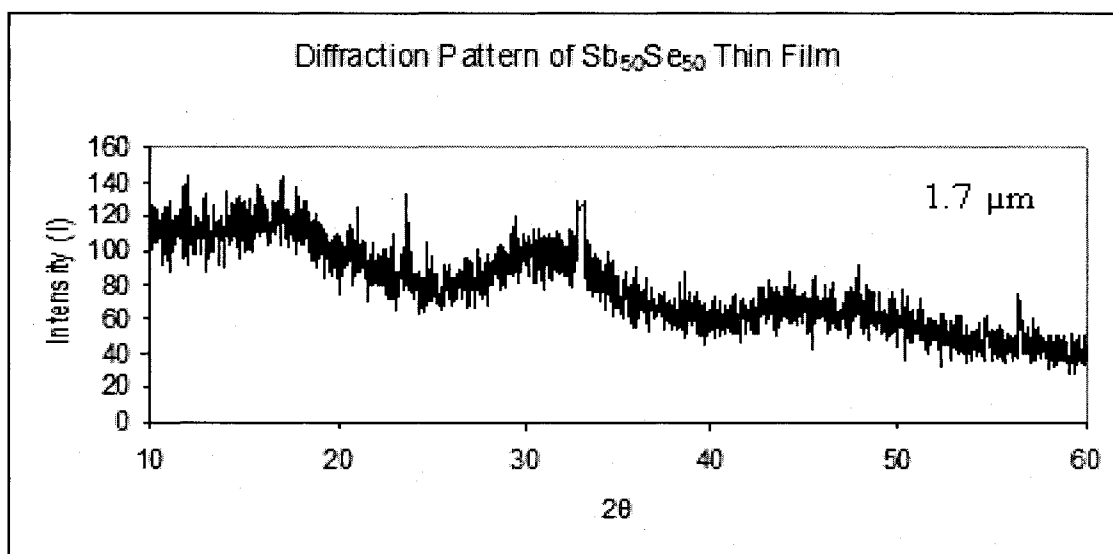


(a)

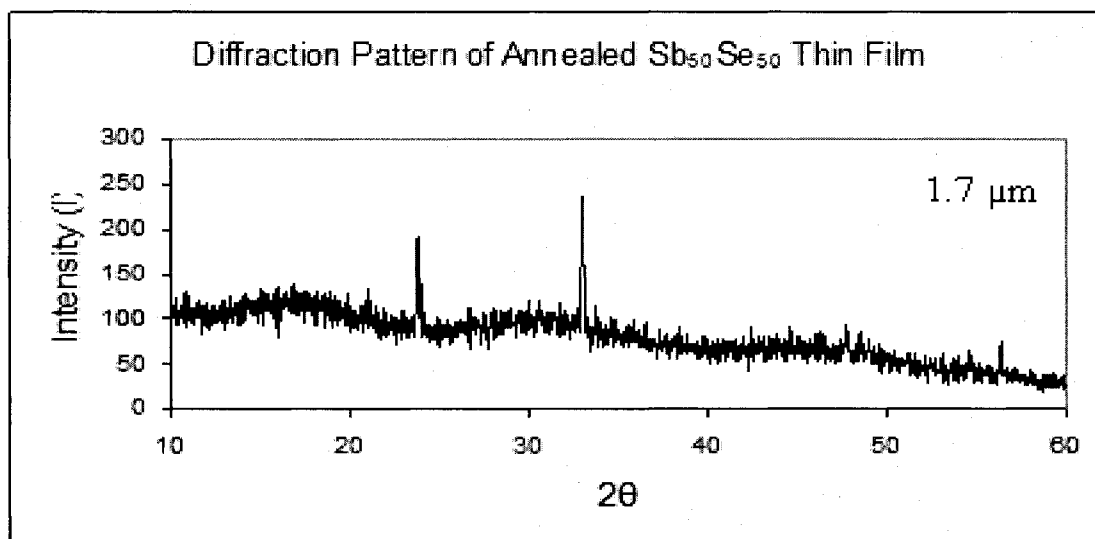


(b)

Figure 4.9 (a) – (b) pre/post annealed X-ray Intensity versus 2 θ plots for $\text{Sb}_{50}\text{Se}_{50}$ thin film of 0.525 μm thickness.

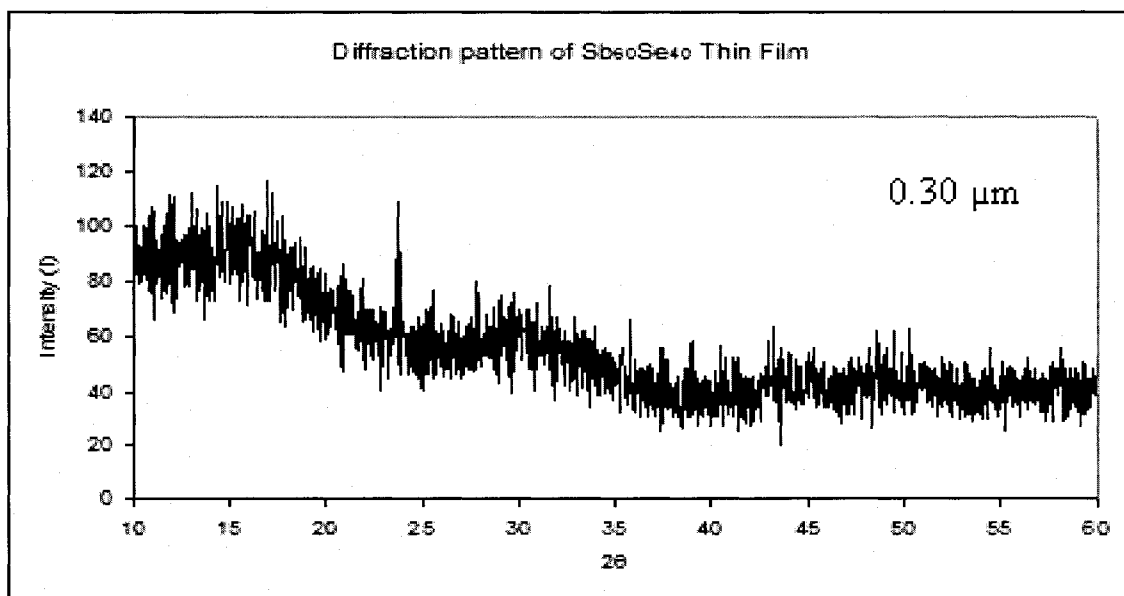


(a)

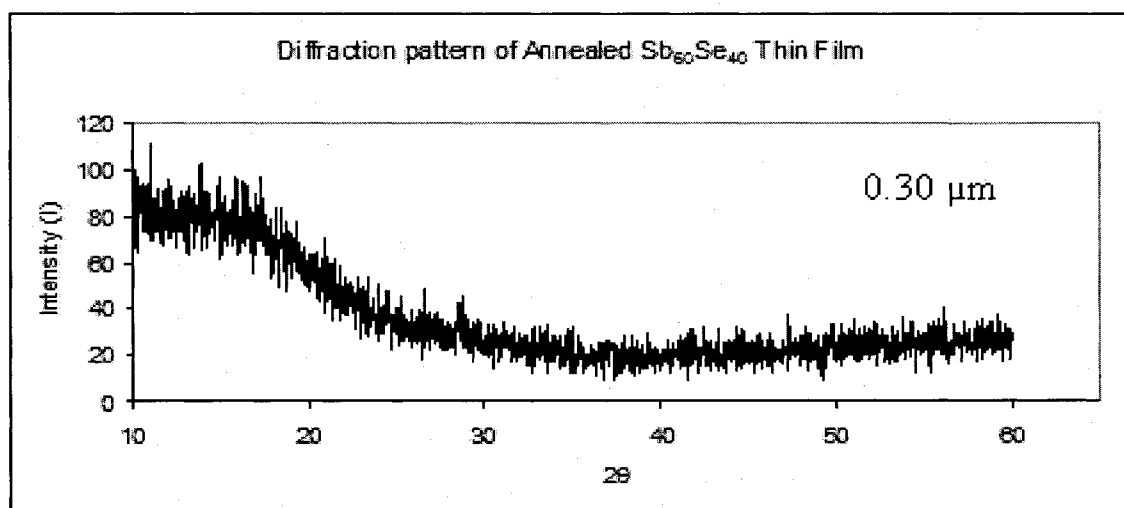


(b)

Figure 4.10 (a) – (b) pre/post annealed X-ray Intensity versus 2θ plots for $\text{Sb}_{50}\text{Se}_{50}$ thin film of 1.70 μm thickness.

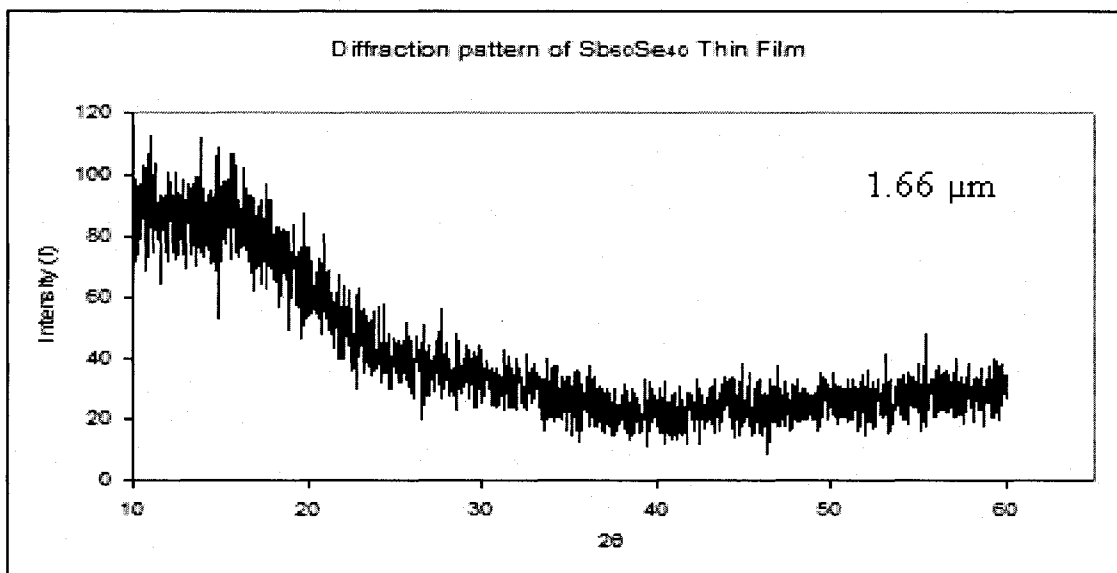


(a)

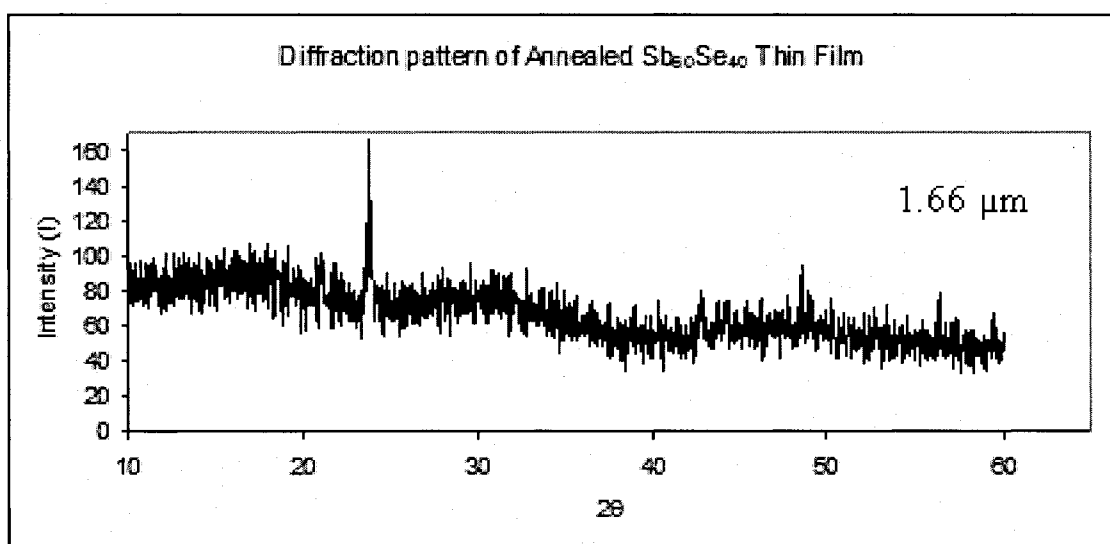


(b)

Figure 4.11 (a) – (b) pre/post annealed X-ray Intensity versus 2 θ plots for Sb₆₀Se₄₀ thin film of 0.30 μm thickness.

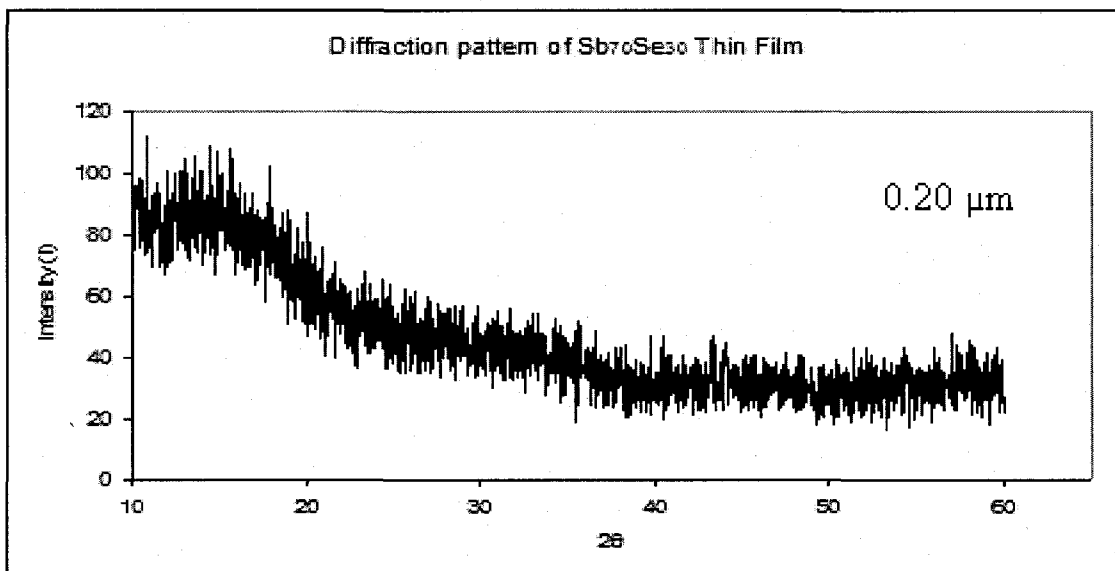


(a)

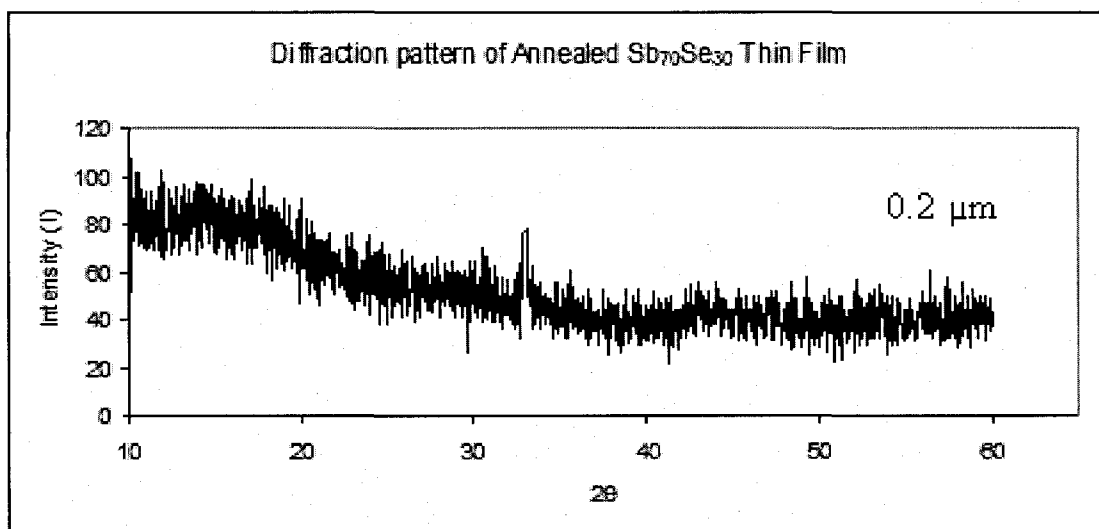


(b)

Figure 4.12 (a) – (b) pre/post annealed X-ray Intensity versus 2θ plots for $\text{Sb}_{60}\text{Se}_{40}$ thin film of 1.66 μm thickness.

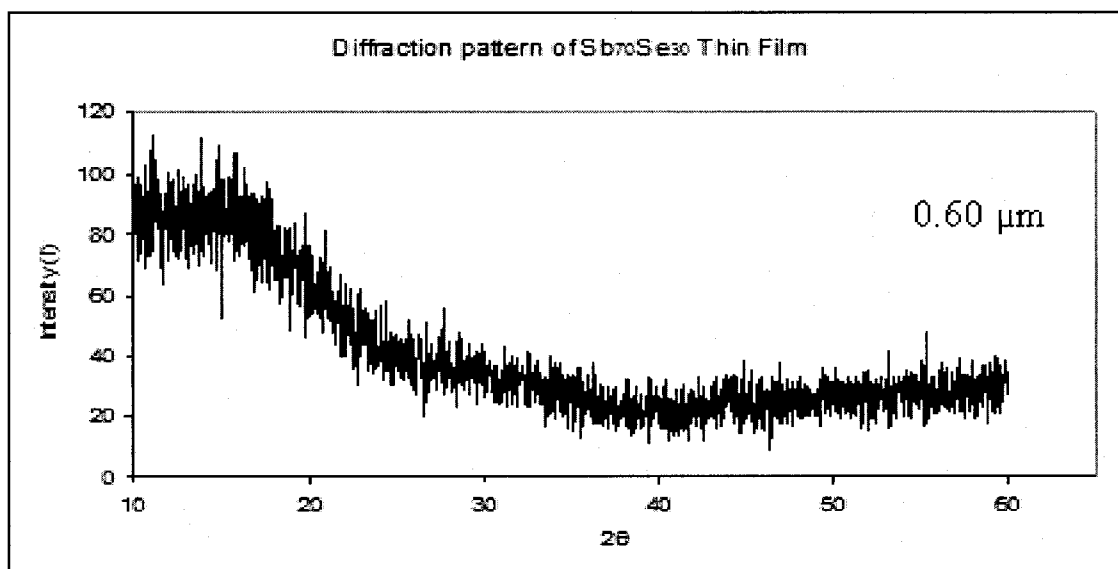


(a)

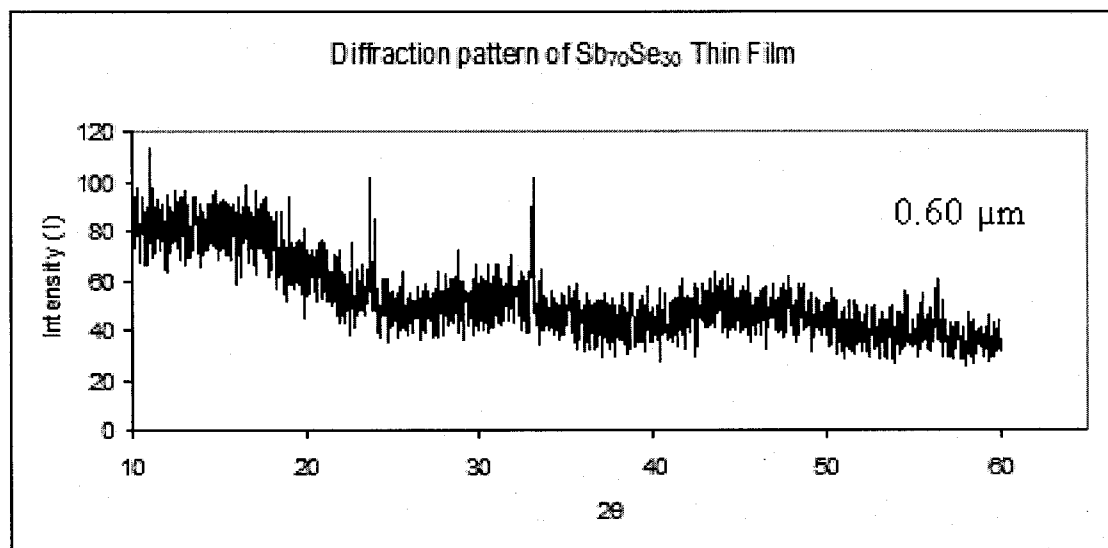


(b)

Figure 4.13 (a) – (b) pre/post annealed X-ray Intensity versus 2θ plots for Sb₇₀Se₃₀ thin film of 0.20 μm thickness.



(a)



(b)

Figure 4.14 (a) – (b) pre/post annealed X-ray Intensity versus 2θ plots for Sb₇₀Se₃₀ thin film of 0.60 μm thickness.

Table 4.5 Pre/Post – annealed optical constants of film samples.

S.No	Compound	Average Refractive Index (n)		Average Extinction Coefficient (k)	
		Pre – Anneal	Post - Anneal	Pre – Anneal	Post - Anneal
1a.	Sb ₄₀ Se ₆₀	3.68	3.44	1.30	1.68
1b.	Sb ₄₀ Se ₆₀	4.06	3.74	1.37	1.43
2a.	Sb ₅₀ Se ₅₀	4.05	3.79	0.97	1.54
2b.	Sb ₅₀ Se ₅₀	4.29	3.75	0.76	1.41
3a.	Sb ₆₀ Se ₄₀	2.88	4.27	1.79	0.54
3b.	Sb ₆₀ Se ₄₀	2.45	4.41	1.69	0.64
4a.	Sb ₇₀ Se ₃₀	3.03	5.36	1.57	0.58
4b.	Sb ₇₀ Se ₃₀	2.83	3.85	1.47	0.60

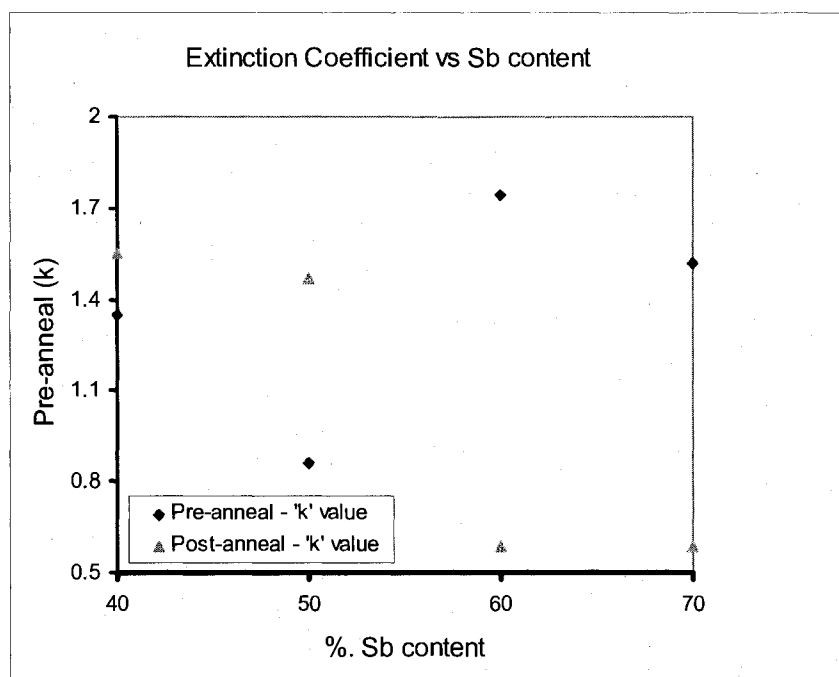
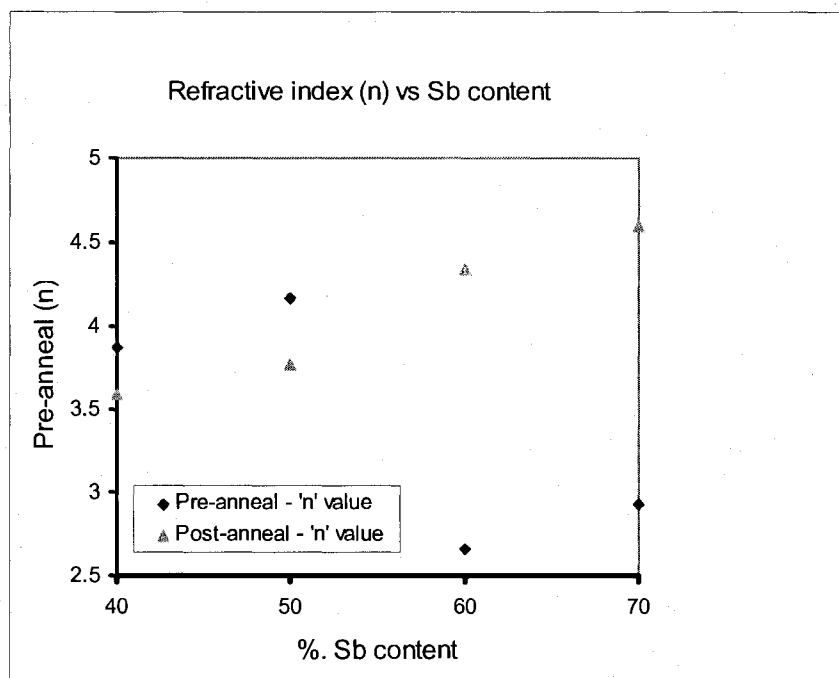


Figure 4.15 Plot of average refractive index (n) and extinction coefficient (k) of pre and post annealed films as a function of Sb content.

From Figure 4.15 shows the variation of average optical constants of thin films before and after annealing as a function of composition. It is found that the average refractive index (n) of annealed films increases from 3.5 at 40% Sb to 4.6 at 70% Sb. Whereas the average extinction coefficient (k) of annealed films decreases from 1.5 to 0.45 and increases slightly to 0.5 beyond 60% of Sb. High refractive index and low extinction coefficient indicates that the thin films tends to behave as a good dielectric material, with low loss factor. Also the difference in average optical constants of thin films of two different thicknesses is less than 10%.

4.1.2.3.3 Electrical Properties

Electrical parameters such as carrier concentration, mobility, and type of conductor of film samples were determined using Hall test equipment. The results obtained are tabulated in the Table 4.6.

Table 4.6 Pre/Post – annealed electrical parameters of thin film samples

S.No	Sample	Carrier concentration (cm ⁻³)		Mobility (cm ² /V/s)		Rh implies	
		Pre	Post	Pre	Post	Pre	Post
1a.	Sb ₄₀ Se ₆₀	3.5X10 ¹⁵	9.0X10 ¹⁵	2.2X10 ²	2.1X10 ²	p	n
1b.	Sb ₄₀ Se ₆₀	6.2X10 ¹⁵	2.3X10 ¹⁶	2.1X10 ²	2.0X10 ²	p	n
2a.	Sb ₅₀ Se ₅₀	2.2X10 ¹⁵	4.5X10 ¹⁶	3.8X10 ²	1.4X10 ²	n	n
2b.	Sb ₅₀ Se ₅₀	8.8X10 ¹⁵	2.9X10 ¹⁶	1.1X10 ²	1.3X10 ¹	n	n
3a.	Sb ₆₀ Se ₄₀	2.4X10 ¹⁶	8.2X10 ¹⁶	5.8X10 ¹	1.1X10 ¹	n	n
3b.	Sb ₆₀ Se ₄₀	7.6X10 ¹⁶	4.1X10 ¹⁷	1.4X10 ¹	1.2X10 ¹	n	n
4a.	Sb ₇₀ Se ₃₀	2.9X10 ¹⁷	6.9X10 ¹⁷	1.6X10 ¹	1.0X10 ¹	n	n
4b.	Sb ₇₀ Se ₃₀	5.2X10 ¹⁷	8.9X10 ¹⁷	1.1X10 ¹	0.95	n	n

From Figure 4.16, it is observed that the number of carriers, i.e., carrier concentration per cm³ in thin films increases with increase in Sb content. This is probably due to the increased semi-metallic nature of the films at higher Sb levels. Also it is found that the carrier concentration of annealed films is greater than that of pre – annealed ones. This is because during annealing process, the atoms in amorphous (pre-annealed) films gain energy and tend to align themselves in a particular pattern (polycrystalline). It is during

this process that the number of charge traps per cm^3 decreases with an associated increase in carrier concentration.

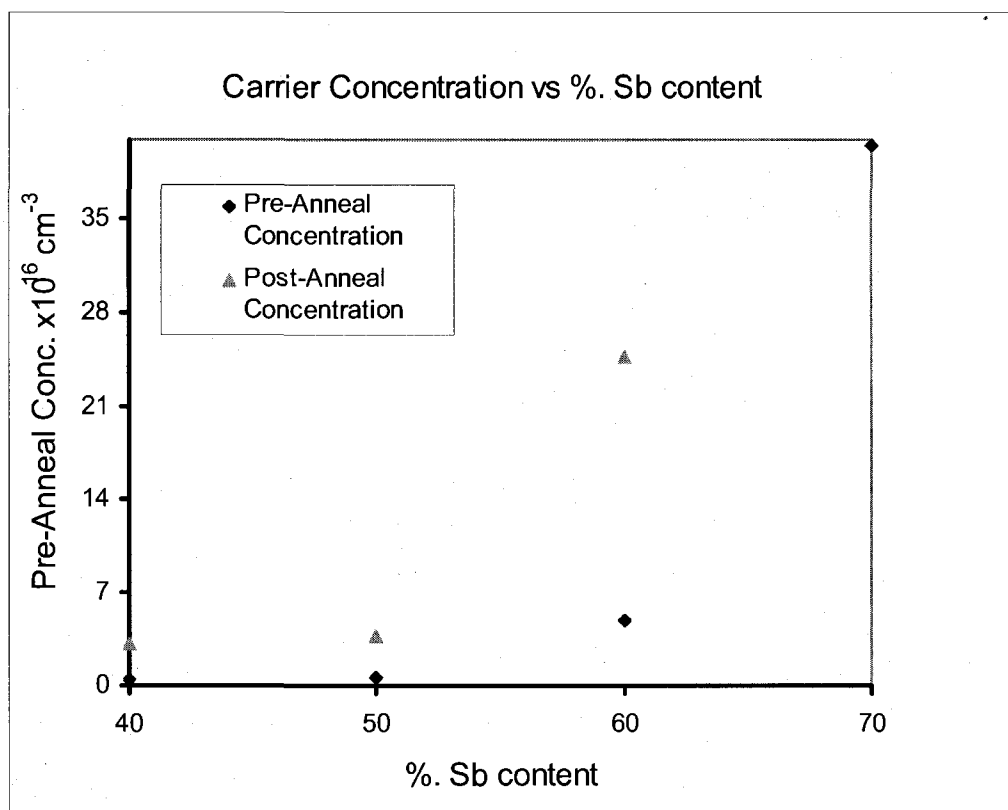


Figure 4.16 Plot of carrier concentration of pre/post annealed films as a function of Sb content.

An increase in carrier concentration is accompanied by decrease in the mobility (μ) of the carriers. This is obvious that as the number of charge carriers increases, the number of scattering events such as, carrier – carrier collisions, carrier – atom collision etc. increases and eventually slowing down the carrier mobility. Figure 4.17 shows the variation of carrier mobility with change in Sb content. Additionally it is found that the

conductivity of $\text{Sb}_{40}\text{Se}_{60}$ thin film upon heating changes from p – type to n – type as shown in Table 4.6. The reason for this switch in conductivity is not obvious.

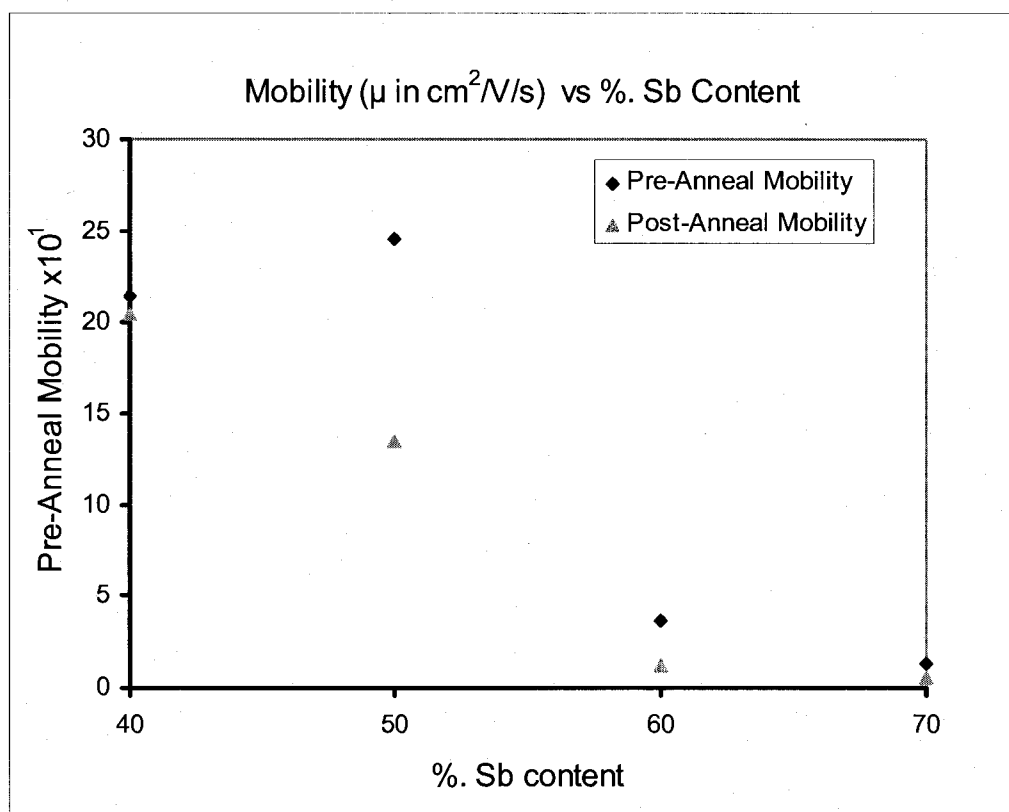


Figure 4.17 Plot of Mobility of pre/post annealed films as a function of Sb content.

4.2 Summary

After performing an extensive study of the structural, electrical, and optical properties of selected compositions of bulk and thin film $\text{Sb}_x\text{Se}_{100-x}$ (for $x = 40, 50, 60, 70$) phase change memory alloys, the following conclusions are drawn.

- The structure of bulk samples is orthorhombic, with compositions being well within the designed values.
- Bulk $\text{Sb}_{55}\text{Se}_{45}$ remains stable without undergoing any chemical or structural decomposition even at temperatures close to 120°C .
- As deposited thin films are amorphous.
- Compositions of thin films are consistent with respect to the bulk, with errors less than 7%.
- Thickness of the deposited films experience $1/d^2$ dependence where 'd' is the distance between the source and the substrate.
- Crystallization temperature (T_c) of thin films increase with increase in Sb content and $\text{Sb}_{40}\text{Se}_{60}$ thin film samples crystallizes at 170°C .
- Refractive index (n) of annealed films increases with increase in Sb content, complementarily Extinction coefficient (k) decreases.
- Carrier concentration of annealed films increases with increase in Sb content, with an associated decrease in carrier mobility.
- Conductivity of annealed $\text{Sb}_{40}\text{Se}_{60}$ thin film samples switches from p-type to n-type.
- The intensity peaks of $\text{Sb}_{40}\text{Se}_{60}$ film of $1\ \mu\text{m}$ thickness are relatively high than the one with $0.65\ \mu\text{m}$ thickness.

CHAPTER 5

CONCLUSIONS AND FUTURE WORK

5.1 Conclusions

Bulk SbSe phase change alloys of varying compositions were synthesized and structural and optical properties of bulk were investigated. The crystal structure of bulk SbSe is found to be orthorhombic at room temperature and results of in-situ X-ray diffraction on bulk $\text{Sb}_{55}\text{Se}_{45}$ show that the bulk remains stable up to 120°C upon heating. Bulk $\text{Sb}_x\text{Se}_{100-x}$ ($40 \leq x \leq 70$) samples were deposited as thin films on Silicon (100) plane substrate using vacuum evaporator system. From XRD analysis, it is found that as deposited thin films are amorphous. The results of compositional analysis on bulk and thin film samples show that the deviation in composition is within 10%. It is observed that thickness of the thin film deposited exhibits a $1/d^2$ dependence where 'd' is the distance between the source and the substrate. Structural analysis on annealed thin films samples show that $\text{Sb}_{40}\text{Se}_{60}$ films crystallize at 170°C and the crystallization temperature (T_c) increases with increase in Sb content of the films. Also it is noticed that for annealed thin films the refractive index (n) increases and extinction coefficient (k) decreases, with increase in Sb content. Hall measurements on pre – annealed and post – annealed films indicate that the carrier concentration of annealed films increases with increase in Sb content, with an associated decrease in carrier mobility (μ). Additionally it is found that the conductivity of $\text{Sb}_{40}\text{Se}_{60}$ samples switches from p-type to n-type upon annealing.

5.2 Future Work

The following are few recommendations for possible future research in this area:

- Depositing thin films with compositions of Sb content lesser than 40% and studying their behavior with respect to crystal structure, electrical, and optical properties upon annealing.
- The quality and uniformity in thickness of the film deposited can be controlled by employing better deposition technique such as DC pulsed or RF Sputtering.
- Measure the resistivity of thin films using four point contact method.
- Design and process Memory Device structures exploiting the low temperature phase transitions.

REFERENCES

- [1] “Phase-change characteristics of chalcogenide $\text{Ge}_1\text{Se}_1\text{Te}_2$ thin films for use in nonvolatile memories”, by Hong-Bay Chung, a_Kyung Shin, and Jae-Min Lee, Korea.
- [2] “Crystallization kinetics of Ga–Sb–Te films for phase change memory”, by Huai-Yu Cheng, Kin-Fu Kao, Chain-Ming Lee, Tsung-Shune Chin.
- [3] “Compact Modeling of Phase-Change Memories”, K. Sonoda, A. Sakai, M. Moniwa, K. Ishikawa, O. Tsuchiya, and Y. Inoue, Japan.
- [4] “Electronic properties of GST for non-volatile memory”, by Hangbing Lva, Peng Zhoua, Yinyin Lina, Tingao Tanga, Baowei Qiaob, Yunfeng Laib, Jie Fengb, Bingchu Caib, Bomy Chenc, USA, 2006.
- [5] <http://www.ovonic.com/>
- [6] <http://news.cnet.com/newsblog/?keyword=%22Gordon+Moore%22>
- [7] “Non-Volatile Random Access Memory Technologies (MRAM, FeRAM, PRAM)”, by Muhammad Muneeb.
- [8] http://www.numonyx.com/Documents/WhitePapers/PCM_Basics_WP.pdf
- [9] “Optical storage”, G.F. Zhou, Mat.Science and Eng., A 304-306 (2001) 73.
- [10] <http://www.tfot.info/>
- [11] <http://ovonyx.com/>
- [12] <http://www.computerworld.com/action/article.do?command=viewArticleBasic>
- [13] “Phase change memories: State-of-the-art, challenges and perspectives”, by A.L. Lacaita

- [14] "Phase-change materials for rewriteable data storage", by Matthias Wuttig and Noboru Yamada, Japan, 2006.
- [15] "Phase-change optical recording: Past, present, future", by A.V. Kolobov, P. Fons, J. Tominaga
- [16] http://en.wikipedia.org/wiki/Phase-change_memory
- [17] "Microchip manufacturing", by Wolf, Stanley.
- [18] "Thin film device applications", by Chopra, Katsuri L.
- [19]
<http://www.corrosionsource.com/technicallibrary/corrdoctors/Modules/MetalCoatings/Physical.htm>
- [20] "Characteristic improvement of $\text{Ge}_1\text{Se}_1\text{Te}_2$ phase change memory by the heating method and the device structure change", by Hyuk Choi, Hyun-Koo Kim, Sang-Mo Koo, Hong-Bay Chung, 2007.
- [21] "Multiple phase-transition in $\text{Ge}_2\text{Sb}_2\text{Te}_5$ based phase change memory cell by current-voltage measurement", by Liangcai Wu, Zhitang Song, Bo Liu, Ting Zhang, Feng Rao, Jie Shen, Feng Wang, Songlin Feng, 2007.
- [22] "Indium selenide (In_2Se_3) thin film for phase-change memory", by Heon Lee, Dae-Hwan Kang, Lung Tran, USA, 2005.
- [23] "Sb-Se-Based Phase-Change Memory Device With Lower Power and Higher Speed Operations", by Sung-Min Yoon, Nam-Yeal Lee, Sang-Ouk Ryu, Kyu-Jeong Choi, Young-Sam Park, Seung-Yun Lee, Byoung-Gon Yu, Myung-Jin Kang, Se-Young Choi, and Matthias Wuttig.

- [24] "Effects of Ge addition on the optical and electrical properties of eutectic $\text{Sb}_{70}\text{Te}_{30}$ films",
by E. Prokhorov, A. Mendoza-Galva'n, J. Gonza'lez-Herna'ndez, B. Chao, 2005.
- [25] "Structural transformation of $\text{Sb}_x\text{Se}_{100-x}$ thin films for phase change nonvolatile memory applications", by M.J. Kang, S.Y. Choi, D. Wamwangi, K. Wang, C. Steimer, and m. Wuttig, 2005.
- [26] <http://epswww.unm.edu/xrd/xrdclass/01-XRD-Intro.pdf>
- [27] http://en.wikipedia.org/wiki/Image:Bragg_diffraction.png
- [28] <http://materials.binghamton.edu/labs/xray/xray.html>
- [29] <http://siliconfareast.com/edxwdx.htm>
- [30] <http://www.angstec.com/Product/SE200.html>
- [31] <http://www.entrepix.com/Veeco/Dektak/Dektak-2-thru-3ST.html>
- [32] <http://hyperphysics.phy-astr.gsu.edu/hbase/magnetic/Hall.html>

VITA

Graduate College
University of Nevada, Las Vegas

Nirup Bandaru

Local Address:

4248 Grove Cir, Apt 3
Las Vegas, NV-89119

Degree:

Bachelor of Technology in Electrical and Computer Engineering, 2006
J.N.T. University, India

Conference Publication:

Title: Synthesis, Structure and Electronic Properties of Phase Change Material $\text{Sb}_{55}\text{Se}_{45}$, Society for the Advancement of Material and Process Engineering (SAMPE), conference, Long Beach, California; May 18 - 22, 2008.

Thesis Title: Synthesis and Characterization of Bulk and Thin film $\text{Sb}_x\text{Se}_{100-x}$ Phase Change Alloys.

Thesis Examination Committee:

Chairperson, Dr. Rama Venkat, Ph. D.
Co-chairperson, Dr. Ravhi S Kumar, Ph. D.
Committee Member, Dr. Paolo Ginobbi, Ph. D.
Committee Member, Dr. Emma Regentova, Ph. D.
Graduate Faculty Representative, Dr. Mohamed B. Trabia, Ph. D.